Facies and stratigraphic architecture of the late Pleistocene to early Holocene tide-dominated paleo-Changjiang (Yangtze River) delta

Xia Zhang[1,2,†], Robert W. Dalrymple[2,†], and Chun Ming Lin[1]

[1]*State Key Laboratory for Mineral Deposits Research, School of Earth Sciences and Engineering, Nanjing University, Nanjing 210023, China*
[2]*Department of Geological Sciences and Geological Engineering, Queen's University, Kingston, Ontario K7L3N6, Canada*

ABSTRACT

This paper reexamines the late Pleistocene to early Holocene transgressive succession (ca. 19.0–8.0 cal. k.y. B.P.) beneath the modern Changjiang delta plain, one of the world's great rivers, by means of a detailed process-oriented investigation of the sedimentary facies and stratigraphic architecture in two newly drilled cores (ZK01 and ZK02), supplemented by correlation with previous work and comparison with the modern deltaic deposits. Results suggest that the study interval, which has previously been considered to have accumulated in an estuary, instead represents a back-stepping delta. The target succession shows a general fining- and muddier-seaward trend for both the channel-bottom and adjacent tidal- or point-bar sediments, from coarse sand and gravels of the purely fluvial channel, through tide-influenced fluvial-channel deposits dominated by medium to coarse sand, to fine-grained sandy or muddy deposits of the (terminal) distributary channels, and finally to prodeltaic mud; the sand-dominated deposits that characterize transgressive estuary mouths are not present. The prodeltaic and delta-front deposits of the paleo- and modern Changjiang deltas display strong similarities, including the pervasive interbedding of tide- and wave-generated fluid-mud deposits and muddy tidal-bar deposits, which are punctuated by terminal-distributary-channel facies that are not expected in an estuary. In more detail, three superimposed successions are recognized, each of which displays an upward-shallowing trend indicating a progradational nature, which is also indicated by the presence of seaward-dipping seismic reflectors in the correlative seaward part of this stratigraphic interval. The three successions show an overall retrogressive, fining-upward trend as a result of stepwise transgression like that seen in the Mississippi and Ganges-Brahmaputra River deltas. This architecture indicates that the large sediment supply of the Changjiang was able to keep pace with or exceed the rate of relative sea-level rise at certain times and locations during the later part of the postglacial transgression. We also propose that the maximum flooding surface occurred at ca. 9.0 cal. k.y. B.P., which is earlier than previously thought; this is also a reflection of the high rate of sediment input of the Changjiang, which causes a turnaround from net transgression to net progradation to occur when the rate of sea-level rise is higher. This study shows that we should not just simply interpret any transgressive succession in an incised valley as estuarine. This study provides significant new insights into the interpretation and sequence-stratigraphic reconstruction of ancient deltaic deposits, and it advances our understanding of the nature of tide-dominated delta successions.

INTRODUCTION

Tide-dominated deltas are arguably the least well-documented type of sedimentary system. They are inherently complex and difficult to study, and relatively little is known about their facies, especially in the shallow subaqueous, delta-front region, despite the fact that a disproportionate number of the world's largest rivers have tide-dominated to strongly tide-influenced deltas (Dalrymple 2010; Goodbred and Saito, 2012). Most modern deltas, including the Changjiang (Yangtze River) delta in eastern China, are the latest phase in the filling of incised valleys that were created during the last glacial lowstand. In such incised-valley-fill successions, the lower part is typically transgressive in character because of accumulation during a period of rapid sea-level rise. These intervals, which are the volumetrically most important component of many incised-valley systems, have recently received significant attention, since they are sensitive recorders of sea level, sediment supply, and climate fluctuations at the land-sea interface, they represent key features for sequence-stratigraphic analyses, and they potentially constitute good oil and gas reservoirs (Dalrymple et al., 1992, 2003, 2012; Allen and Posamentier, 1993; Lin et al., 2004, 2005, 2010; Boyd et al., 2006; Tessier, 2012; Zhang et al., 2013, 2014, 2015; Feng et al., 2016). These transgressive successions most commonly consist of deposits that formed in an estuarine environment (sensu Dalrymple et al., 1992, 1994; Allen and Posamentier, 1993; Thomas and Anderson, 1994; Zhang et al., 2014), but they can alternatively consist of aggradational or back-stepping, progradational deltaic lobes (Fisk and McFarlan, 1955; Goodbred and Kuehl, 2000a, 2000b), depending on the balance between accommodation and riverborne sediment supply (Catuneanu, 2006).

The Changjiang (Yangtze River), ranked as the world's fifth largest river with respect to water discharge and the fourth globally in terms of average suspended sediment load, has formed an ~90-m thick-postglacial incised-valley-fill succession, which is the primary host of shallow biogenic gas in eastern China, with the gas occurring especially in the sediments located on the northern margin of the modern Changjiang delta plain (Wang, 1982; Zheng, 1998). Nevertheless, exploration for gas reserves therein has not achieved a major breakthrough after >60 yr of research and development. The late Pleistocene to early Holocene transgressive succession, which occupies ~65% of the total volume of the incised-valley succession (Li et al., 2006), has inevitably become the main exploration target and has been studied extensively based on numerous cores located in the modern delta plain and seismic profiles in the present-day

†Corresponding authors: zhangxiananjing@163.com; dalrympl@queensu.ca.

subaqueous delta area (Hori et al., 2001a; Li et al., 2000, 2002; Chen et al., 2003; Wang et al., 2007, 2012a; Liu et al., 2010; Fan et al., 2011; Song et al., 2013; Feng et al., 2016; Xu et al., 2016, and references therein). Although there is a common belief that these deposits accumulated in a tide-dominated estuary, several characteristics of the succession, including a seaward-fining trend in the bulk grain size and the presence of seaward-dipping seismic reflections (Hori et al., 2001a; Feng et al., 2016; Xu et al., 2016), are inconsistent with this interpretation and potentially indicate that it may instead be deltaic in origin. The current lack of understanding of the true nature of these deposits seriously hinders the exploration for shallow biogenic gas reservoirs, because the spatial and temporal distribution of sedimentary facies is very different between the two types of systems as a result of the different sediment-transport pathways and physical processes (Dalrymple et al., 1992, 2012; Dalrymple and Choi, 2007; Goodbred and Saito, 2012; Chen et al., 2015). In addition, the heterolithic nature of tide-dominated successions resulting from the cyclic variation of tidal-current strength increases the lateral and vertical heterogeneity of the reservoirs; indeed, tidal-channel deposits, the likely reservoir facies for biogenic gas, can locally serve either as baffles or reservoirs, depending on sand content (Feldman and Demko, 2015). Consequently, the late Pleistocene to early Holocene transgressive succession in the postglacial Changjiang incised valley requires significant additional detailed investigation.

This study is an extension of previous work, and it is the first comprehensive process-based investigation of the deposits at the level of individual layers, focusing especially on the characteristics of the muddy deposits within the late Pleistocene to early Holocene transgressive succession recovered in two newly drilled cores (ZK01 and ZK02), combined with correlation with previously published cores and seismic profiles from the study area. The main goals of the investigation were to: (1) interpret the origin of the various types of mud layers; (2) interpret the nature of the depositional subenvironments present based on the character of the mud and sand layers; (3) document the vertical facies succession in more detail than has been done in the past; and (4) discuss the controls on the evolution of this succession. This study sheds new insights on sedimentation in the fluvial-tidal transition zone during an overall transgressive interval, facilitating the environmental interpretation and sequence-stratigraphic reconstruction of similar ancient deposits. It also provides more, badly needed documentation of the deposits of a tide-dominated delta. In the local

context, the results will be of great importance for predicting the distribution of reservoir facies and guiding the exploration for shallow biogenic gas in the study area.

GEOLOGICAL BACKGROUND

Environmental Setting

The modern Changjiang delta is situated in a zone of coastal subsidence, with a subsidence rate of 1–2 mm/yr (Li et al., 2002), and the altitude of the delta plain is generally <5 m above mean sea level (Stanley and Chen, 1996). It is bounded by hills in the west (Fig. 1), and it slopes gently toward the east over a distance of ~250 km from the Zhenjiang-Yangzhou area, which is the location where the river enters the coastal plain and the most landward position of the delta apex at the end of the postglacial transgression (Hori et al., 2001a; Li et al., 2002; Song et al., 2013). The modern Changjiang delta covers an area of ~5.2×10^4 km^2, with 2.3×10^4 km^2 being subaerial and 2.9×10^4 km^2 subaqueous (Li et al., 2002). It has been constructed by the Changjiang (Yangtze River), which is one of the world's great rivers, with a water discharge of 924 km^3/yr and an annual sediment discharge of 5.0×10^{11} kg/yr (Milliman and Syvitski, 1992). The discharge shows pronounced variations between dry and wet seasons, with ~70% of the annual freshwater discharge and 87% of the annual suspended-sediment discharge occurring in the flood season (June to September; Shen et al., 1992; Shen and Pan, 2001; Shi, 2004). Broadly similar discharge characteristics are thought to have existed throughout the Holocene, although century-scale fluctuations are thought to have occurred as a result of climate changes in the source area (cf. Hori et al., 2002a, 2002b; Chen et al., 2005; Tao et al., 2006; Yi et al., 2006; Wang et al., 2010).

The tide in the modern Changjiang delta is semidiurnal, with a mean tidal range of ~2.7 m and a maximum tidal range that reaches 4.6 m during spring tides near the river mouth (Shen et al., 1988). The average tidal-current speed is on the order of 1.0 m/s (Shen et al., 1988), but the maximum ebb and flood tidal-current velocities can exceed 2.0 m/s and 1.5 m/s during spring tides, respectively; the corresponding values during neap tides are 1.5 m/s and 1.0 m/s (Chen et al., 1988). In general, the ebb tidal-current velocity is faster than that of the flood tide within the channels, whereas the flood tidal-current speeds (0.21–0.35 m/s) are faster than those of the ebb tide on the tidal flats (Fan and Li, 2002). Both the tidal range and tidal-current velocity decrease landward (Wu et al., 2012). The tidal influence can, however, reach up to

230 km upstream (around Yangzhong) from the river mouth during the dry season, but only 150 km upstream (near Jiangyin) during the river-flood season (Li et al., 1983; see locations in Fig. 1). Numerical simulations of the tides indicate that they have been approximately the same as today throughout the latter part of the postglacial transgression (Uehara et al., 2002), and sedimentation is thought to have been tide-dominated over this entire period (cf. Hori et al., 2001a, 2002a, 2002b; Li et al., 2000, 2002, 2006; Feng et al., 2016; Xu et al., 2016).

Wave action has a lesser influence on sedimentation but cannot be ignored in the exposed outer part of the modern delta. The general wind pattern consists of prevailing southeasterly winds during the summer and northwesterly winds in the winter (Li and Wang, 1998). Although directed onshore, the summer winds are generally weak and do not generate large waves. The winter winds are stronger but are directed offshore, so they also do not generate intense wave action. Tropical cyclones, on the other hand, are accompanied by very strong wave action that has an intense impact on China's coast on an annual basis. Indeed, in an average year, seven typhoons make landfall on the coast, generally to the south of the modern Changjiang delta, generating large waves for periods ranging from several days to more than 2 wk (Fan et al., 2006). The mean and maximum wave heights near the river mouth are 0.9 m and 6.2 m, respectively (Zhu et al., 1988; Li and Wang, 1998; Fan et al., 2006), and the mean effective depth of wave action varies seasonally from 2 m to 6 m below mean sea level (Zhu et al., 1988).

The modern delta exhibits the classic morphology of a tide-dominated system, with multiple, funnel-shaped distributary channels that are separated by shore-normal elongate islands and subaqueous shoals (i.e., elongate tidal bars); a similar morphology is believed to have existed throughout the period of interest in this study. Unlike the Fly and Han River deltas, in which the channels bifurcate from a common point (Dalrymple et al., 2003; Cummings et al., 2015), the bifurcations in the Changjiang delta occur sequentially. The first bifurcation (i.e., "the apex" of the modern Changjiang delta) occurs ~90 km from the coast, where the main channel splits into the North and South Branches, separated by Chongming Island and its seaward extension, Chongming Shoal, on the delta front (Fig. 1). The main Changjiang channel occupied the North Branch during the fourteenth to seventeenth centuries, but then it switched to the South Branch in the eighteenth century (Xu et al., 2016). At present, ~98% of the river runoff is debouched through the South Branch, and the North Branch only discharges
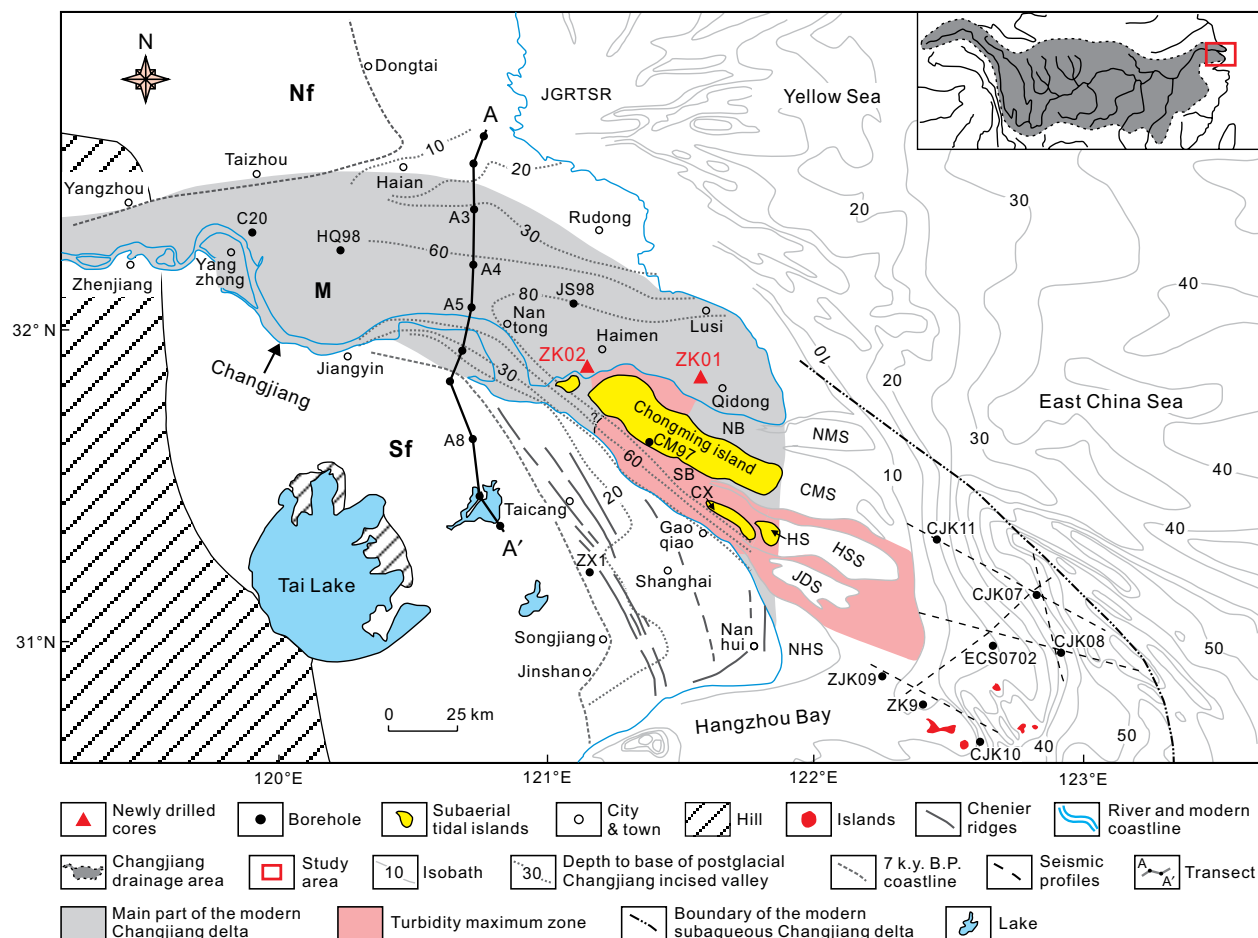
Figure 1. Sketch map of the modern Changjiang delta and the adjacent part of the East China Sea and Yellow Sea continental shelf, showing the basal topography of the Changjiang incised valley around the time of the Last Glacial Maximum (dotted lines on land), bathymetry, as well as the locations of chenier ridges, turbidity maximum zone, newly drilled cores ZK01 and ZK02, correlative boreholes, core transect, and seismic profiles (modified from Shen et al., 1992; Hori et al., 2001a; Li et al., 2002; Xu et al., 2016). Bathymetric contour interval is 5 m. Although the documented turbidity maximum zone is located in the mouth area of the South Branch, it extends farther landward, especially during the river-flood season, when large quantities of suspended sediments are debouched into the distributary channels. M—main delta (last glacial incised-valley area); Sf—southern flank; Nf—northern flank; JGRTSR—Jianggang radial tidal sand ridges; NB—North Branch; SB—South Branch; CMS—Chongming Shoal; HSS—Hengsha Shoal; HS—Hengsha Island; CX—Chongxing Island; NHS—Nanhui Shoal; JDS—Jiuduan Shoal; NMS—northern margin shoal. A-A′ = location of cross section shown in Figure 2.

river water during low tides in flood seasons. The South Branch undergoes a further bifurcation ~30 km from the coast, forming the North and South Channels, separated by Changxing and Hengsha Islands and their subaqueous extension, Hengsha Shoal. These channels extend across the subaqueous delta platform (the delta-front region), with the South Channel splitting again into the North and South Passages, which are separated by Jiuduan Shoal (Fig. 1). The North Branch also bifurcates on the subaqueous delta platform, with the northern-margin shoal lying between them.

The subaqueous part of the delta can be subdivided into the delta-front (0 to ~15 m depth) and prodelta (15–30 m depth) areas. The former

consists of "subtidal flats" (shoals or tidal bars) with water depths <5–10 m that are separated by tidal channels that are the seaward extension of the distributary channels. The relief between the shoal crests and channel axes decreases seaward from ~5–15 m at the coast until the channels end 40–60 km seaward of the coast in a water depth of ~15 m (for more details about the river-mouth bathymetry, see Wang et al., 2007). The prodelta is, therefore, generally unchannelized. Beyond the toe of the prodelta, series of relict transgressive sand ridges are present in water depths >30 m (Fig. 1; Chen et al., 2000; Berné et al., 2002; Uehara et al., 2002). The sand discharged by the Changjiang accumulates dominantly in the subaerial delta-plain and delta-front areas,

in water depths <10 m, whereas the mud is deposited in the delta front and prodelta, or it is transported southeastward into the nearby Hangzhou Bay or along the Zhejiang-Fujian coast to form a coastal mud wedge (Chen et al., 2000; Zhang et al., 2014, 2015).

Suspended-sediment concentrations in the modern Changjiang delta are constantly high because of the huge content (>95% of the total sediment load) of fine-grained sediments (<63 μm) supplied by the river (Shi et al., 2006), and the strong resuspension of previously deposited sediment by waves and tidal currents. The suspended-sediment concentrations do, however, show significant temporal and spatial variations. They vary seasonally throughout the

delta, being higher during the river-flood season and lower in the dry season, as a result of the seasonal variation in river discharge. The suspended-sediment concentrations near the bed are commonly >3.0–4.0 g/L and can instantaneously reach up to >40 g/L during the river-flood season, but they are generally lower than 0.5 g/L during the dry season (Shen et al., 1992; Shi, 2004; Wang et al., 2007). In the seaward part of the delta, however, this pattern is complicated by episodically intense, wave-induced resuspension during the winter and during typhoons. Tidal-current resuspension also generates a pronounced neap-spring cyclicity, with suspended-sediment concentrations generally higher during spring tides and lower during neap tides (Chen et al., 2006; Wu et al., 2012; Yang et al., 2014; Yang and Yang, 2015). Spatially, the suspended-sediment concentrations are highest in the turbidity maximum zone, the peak of which in the modern Changjiang delta lies in the mouth area of the South Branch and near the modern "apex" in the "abandoned" North Branch (Shen et al., 1992; Fig. 1). This turbidity maximum zone extends for a range of 25–46 km and moves seawards ~10 km during the river-flood season (cf. Shen et al., 2003). In the turbidity maximum zone, the suspended-sediment concentrations are generally in the range of 0.1–0.7 g/L 0.5–1.0 m below the water surface and 1–10 g/L near the bed (0.2–1.0 m above the channel bottom; Milliman et al., 1985; Shen et al., 1992; Li et al., 1994; Li and

Zhang, 1998; He et al., 2001; Shi et al., 2006). Thick soupy fluid-mud layers (commonly of 0.2–0.6 m thick, reaching up to 1.0–1.2 m), in which the suspended-sediment concentrations can reach 1040 g/L at the top of mud layer and 1250 g/L at the bottom, can form near the bed in the turbidity maximum zone during the river-flood season or after storms (Shen et al., 1992).

Sea-Level History

Sea level fell to about –135 m in the East China Sea during the Last Glacial Maximum (LGM), resulting in the whole continental shelf being exposed (Zhu et al., 1979; Li et al., 2014). After the lowstand, sea level rose rapidly from ca. 19.0 cal. k.y. B.P. to 7.0 cal. k.y. B.P. This period was, however, characterized by four phases of especially rapid rise (RRPs I, II, III, and IV) and two phases when the rate of rise was slower (SRP I and II; see fig. 2 *in* Li et al., 2014). RRP I (19.0–18.5 cal. k.y. B.P.) resulted from the rapid melt of the ice cap at the end of the LGM, with a mean rate of rise of 20 mm/yr. SRP I (18.5–15.4 cal. k.y. B.P.) was caused by Henrich event 1 (Rühlemann et al., 1999; Deschamps et al., 2012) and the Older Dryas (Koutavas et al., 2002) cooling events, during which sea level rose at a mean rate of 5 mm/yr. RRP II (15.4–12.9 cal. k.y. B.P.) was the result of meltwater pulse 1a and the Bølling-Allerød (BA) and Termination-1a warming events (Deschamps et al., 2012; Li et al., 2014), and

it had a mean rate of rise of 15 mm/yr. SRP II (12.9–11.0 cal. k.y. B.P.) was the response to the Younger Dryas cooling event (Rühlemann et al., 1999; Koutavas et al., 2002; Bard et al., 2010), during which sea level rose at a mean rate of 6 mm/yr. RRP III (11.0–9.3 cal. k.y. B.P.) was generated by meltwater pulse 1b, accompanied by the Termination-1b warming event, and it had a mean rate of rise of 17 mm/yr (Fairbanks, 1989; Rühlemann et al., 1999). RRP IV (9.3–7.0 cal. k.y. B.P.), during which sea level rose at a rate of 11 mm/yr, was mildly influenced by the so-called 8.2 ka event (Hijma and Cohen, 2010; Tjallingii et al., 2014, and references therein). Since the end of RRP IV, sea level has been approximately stable at its present level, rising less than 1 mm/yr.

Stratigraphic Architecture of the Postglacial Succession

The Changjiang incised valley that was formed during that last glacial lowstand period lies beneath the main part of the modern Changjiang delta (Hori et al., 2001a; Li et al., 2000, 2002; Fig. 1). It is up to 70 km wide, and its base lies ~80–90 m below present sea level at the modern river mouth, whereas the sequence boundary on the interfluves is located ~20–30 m below present sea level (Fig. 2). The facies characteristics, stratigraphic architecture, environmental evolution, and accumulation rates of the postglacial Changjiang incised-valley fill have
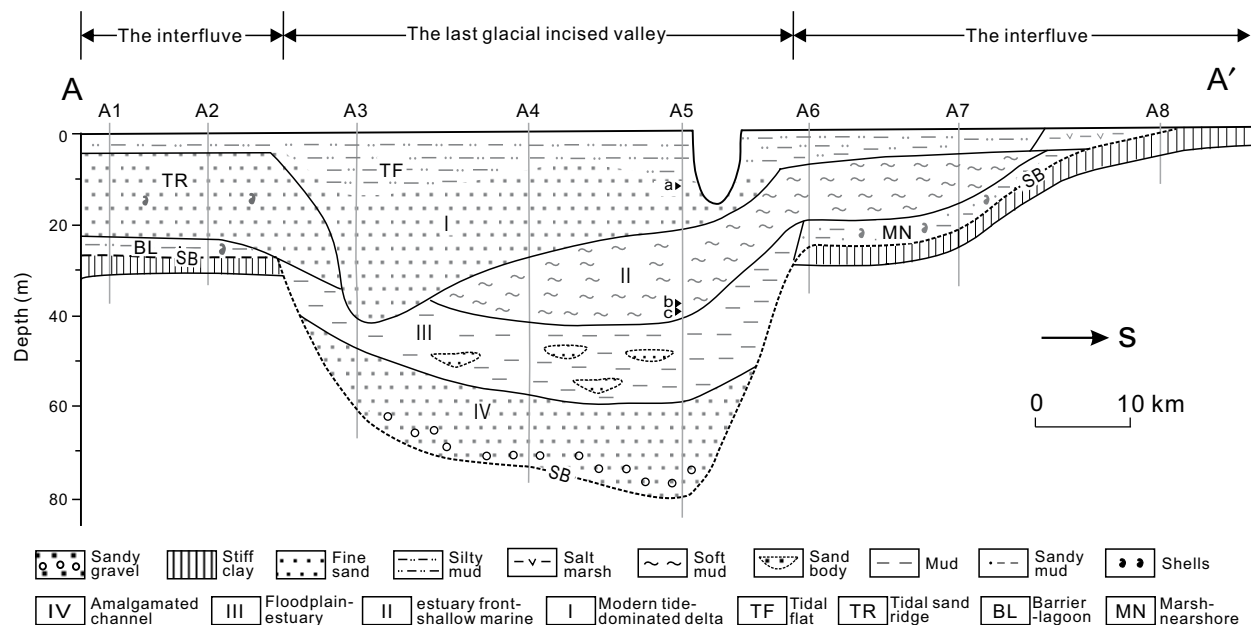
Figure 2. North-south stratigraphic transect (A-A′; see location in Fig. 1) across the modern Changjiang delta region (modified from Li et al., 2006). The environmental interpretations of units II and III are the primary focus of this paper. SB—sequence boundary. ¹⁴C data are derived from Li et al. (2002): a—6595 ± 320 cal. yr B.P., 11.70 m depth; b—11,490 ± 930 cal. yr B.P., 35.5 m depth; c—12,900 ± 190 cal. yr B.P., 38.80 m depth (Table 1).

been studied extensively based on the analysis of more than 600 boreholes drilled in the modern Changjiang delta plain, as well as >20 cores and a number of high-resolution seismic profiles in the subaqueous delta-front and prodelta areas (Li et al., 2000, 2002, 2006; Chen et al., 2000, 2003; Hori et al., 2001a, 2002a, 2002b; Wang et al., 2007, 2012a; Liu et al., 2010; Song et al., 2013; Li et al., 2014; Feng et al., 2016; Xu et al., 2016, and references therein). The chronological framework is constrained by hundreds of radiocarbon (accelerator mass spectrometry [AMS] ^{14}C) dates on molluscan shells, foraminifera, bivalve shells, wood, and other plant material, including peat (Li et al., 2000, 2002, 2006; Hori et al., 2001a, 2002a, 2002b; Xu et al., 2016, and the references therein), and a smaller number of optically stimulated luminescence dates (Xu et al., 2016). In general, the incised-valley fill consists of three main depositional systems (Fig. 2): fluvial deposits of the lowstand systems tract (LST) and early transgressive systems tract (TST; from the LGM at 19.0 cal. k.y. B.P. to 13.4 cal. k.y. B.P.), with the initial flooding surface lying within these river deposits; late transgressive deposits (13.4–8.0 cal. k.y. B.P.) that are traditionally interpreted to represent a tide-dominated estuary (sensu Dalrymple et al., 1992); and the modern regressive tide-dominated delta (after ca. 8.0 cal. k.y. B.P.). These facies accumulated during the postglacial sea-level rise and the subsequent stillstand, indicating a period of deepening and transgression followed by shallowing and progradation (Fig. 2). The sediments of the transgressive tide-dominated interval are the target of this study.

MATERIALS AND METHODS

In 2014, two new cores, ZK01 (112 m penetration depth, 0.1 m diameter) and ZK02 (128 m penetration depth, 0.1 m diameter), were collected from the Qidong (31°50′26.74″N, 121°33′24.08″E) and Haimen (31°52′47.12″N, 121°09′30.69″E; Fig. 1) areas, respectively, by rotary drilling. They penetrated the entire postglacial succession described herein, with a recovery in both cores of more than 90%. In the laboratory, these cores were split, photographed, described, and subsampled. The sedimentological characteristics documented included grain size, sorting, layer thickness, nature of the contacts between the sand and mud layers, sedimentary structures, and ichnology. The grain size of 134 samples (0.5–1.0 m spacing) was analyzed at 0.25Φ intervals using standard methods (cf. Zhou and Gao, 2004), with grain-size parameters determined using the GRADISTAT software (Blott and Pye, 2001). Ten samples were obtained for gastropod-fossil

identification using the method described by Yu et al. (1963). Forty-three samples were collected for determination of the foraminifer content using the method described by Zhang et al. (2014) and Wang et al. (1988). The ^{14}C ages were determined on shells, organic-rich sediments, and plant material by the Beta Analytic Radiocarbon Dating Laboratory, Miami, Florida, USA (Lab No. Beta; Table 1) using AMS dating. In this paper, AMS ^{14}C ages were calibrated using the Calib Rev 7.1 (beta) program (Reimer et al., 2013); the ^{14}C ages of four shell samples were calibrated utilizing the Marine13 model with a ΔR value of 135 ± 42 to deal with the marine reservoir effect (cf. Yoneda et al., 2007; Wang et al., 2012a). We also collected AMS ^{14}C dates previously determined from cores HQ98, CM97, JS98, ZK9, CJK07, CJK11, and A5 (see locations in Fig. 1; Hori et al., 2001a; Li et al., 2002; Wang et al., 2010) and converted them to calibrated ages (Table 1). Sedimentary logs of the two cores showing the results obtained are provided in Figure 3.

RESULTS

Most of the late Pleistocene to early Holocene transgressive deposits (15.4–8.0 cal. k.y. B.P.) are heterolithic, with interstratification of sand or coarse silt and mud (silt and/or clay) on scales ranging from millimeter-thick laminae to decimeter-thick beds (Figs. 3–7). Detailed examination reveals that most sand layers in the cores appear structureless, which is probably due to the narrow range of grain sizes, the thinness of layers, and/or disturbance by coring; crude cross-stratification, parallel lamination, and ripple lamination can be seen only in some places. Thus, the facies scheme and environmental interpretation developed for these deposits rely heavily on the features of the pervasive and diverse mud deposits. Despite the widespread presence of mud or mudstone layers in tide-dominated deposits of all types, they have generally not received significant attention in facies analyses, even though they have enormously variable sedimentary characteristics and invaluable environmental implications (cf. Traykovski et al., 2000; Gabioux et al., 2005; Hill et al., 2007; Ichaso and Dalrymple, 2009; Mackay and Dalrymple, 2011; Hale and Ogston, 2015). A comprehensive understanding of the physical processes responsible for the formation of the mud layers in coastal successions is of particular significance in accurately interpreting sedimentation processes and the associated environmental setting, in particular, because they can provide important insight into the spatial and temporal variations of suspended-sediment concentrations, and

the location and magnitude of the turbidity maximum zone, which are in turn controlled by the relative intensities of tidal, fluvial, and wave processes (Shen et al., 1992; Jaeger and Nittrouer, 1995; Doxaran et al., 2009; Mackay and Dalrymple, 2011; Wu et al., 2012). For these reasons, we focus first on the attributes of the mud layers in the following analysis of the late Pleistocene to early Holocene transgressive deposits. The terminology used to classify layer thickness follows Collinson and Thompson (1989) and Mackay and Dalrymple (2011). The term "layer" is used to refer to a lithologically homogeneous unit of any thickness, and "bed" is used for layers thicker than 1 cm, whereas those <1 cm thick are "laminae." To permit a finer-scale terminology for bed thickness, thin beds are layers with thicknesses of 1–5 cm, and thick beds are >5 cm thick.

Mud-Layer Analysis

Mud layers are pervasive within the late Pleistocene to early Holocene transgressive deposits and have widely variable characteristics. The individual layers range from 0.1 cm to 30 cm thick, can be homogeneous or internally stratified, can have sharp or gradational upper and lower contacts, and can be weakly to moderately bioturbated (i.e., bioturbation index [BI] of 0–3), with the bioturbation most commonly extending downward from the top of a layer (Fig. 4). Two types of mud layers recur in the cores based on the vertical variation in layer thickness (Table 2): organized mud layers (OM; i.e., tidal rhythmicity is evident; Figs. 4A–4D) and disorganized mud layers (DM; tidal rhythmicity is not present, and the layers occur "randomly"; Fig. 4E).

The OM style of layering consists of lithologically structureless mud laminae or beds that can have abrupt or gradational contacts with the over- and underlying sand layers (Table 2; Figs. 4A–4D). It is referred to as organized because the deposits commonly occur interlaminated or interbedded with sand or coarse silt, the layers of which display regular variations in thickness, generating cyclic thick-thin layers and gradational alternations between sandier and muddier intervals (Table 2; Figs. 4A–4C). The OM layering can be subdivided into two types (Table 2). The organized-mud type 1 (OM1) contains mud layers with thicknesses <1 cm that are weakly or moderately bioturbated (BI 0–3), and that locally show obvious sandier-muddier cyclicity (Table 2; Figs. 4A and 4B). The organized-mud type 2 (OM2) is characterized by thicker mud layers (typically 1–5 cm thick) that have sharp bases and layer tops that display small load structures and

TABLE 1. ACCELERATOR MASS SPECTROMETRY (AMS) ¹⁴C AGES OF ORGANIC SEDIMENTS, PLANT MATERIALS, WOOD, FORAMINIFERA, AND SHELL SAMPLES FROM THE NEWLY DRILLED ZK01 AND ZK02 CORES, AS WELL AS PREVIOUSLY PUBLISHED CORES IN THE MODERN CHANGJIANG DELTA AREA

Lab. code	Depth (m)	Material	δ¹³C (‰)	Measured ¹⁴C age (yr B.P.)	Conventional ¹⁴C age (yr B.P.)	Calibrated ¹⁴C age (cal. yr B.P.) Age (1σ)	Prob.	Age (2σ)	Prob.	Notes	References
ZK01											
Beta-409604	29.9	Organic sediment	−24.5	5500 ± 30	5510 ± 30	6300 ± 18	0.95	6310 ± 40*	0.83	Modern delta	This study
Beta-409605	34.6	Shell	−0.8	3800 ± 30	4200 ± 30	4090 ± 85	1	4100 ± 165	1	Modern delta	This study
Beta-409606	60.0	Organic sediment	−23.0	11,080 ± 40	11,110 ± 40	13,000 ± 60	1	12,960 ± 120	1	S1	This study
Beta-409607	75.6	Shell	−2.0	11,790 ± 60	12,170 ± 60	13,470 ± 90	1	13,500 ± 180	1	F2	This study
Beta-409608	82.6	Shell			>43,500					Basement	This study
ZK02											
Beta-424783	30.6	Shell	−0.6	4220 ± 30	4620 ± 30	4690 ± 80	1	4670 ± 140	1	Modern delta	This study
Beta-409611	31.8	Shell	−3.0	6790 ± 30	7150 ± 30	7510 ± 50	1	7500 ± 90	1	Modern delta	This study
Beta-424784	46.3	Plant material	−28.6	8450 ± 30	8390 ± 30	9440 ± 30	1	9440 ± 45	0.82	S2	This study
Beta-409612	47.1	Shell	−8.4	10,680 ± 40	10,950 ± 40	12,780 ± 45	1	12,820 ± 110*	1	S2	This study
Beta-424785	51.6	Organic sediment	−24.5	1,0680 ± 40	10,690 ± 40	12,670 ± 40	1	12,650 ± 70	1	S1	This study
Beta-424786	65.3	Plant material	−29.0	11,490 ± 40	11,420 ± 40	13,340 ± 50	1	13,350 ± 90	1	F2	This study
Beta-424788	84.9	Organic sediment	−20.9	33,510 ± 220	33,580 ± 220	38,050 ± 360	1	37,840 ± 730	1	Basement	This study
A5											
	11.7	Organic sediment			5750 ± 150	6560 ± 160	1	6595 ± 320	1	Modern delta	Li et al. (2002)
	35.5	Organic sediment			9900 ± 300	11,520 ± 450	0.92	11,490 ± 930	1	S1?	Li et al. (2002)
	38.8	Organic sediment			11,030 ± 123	12,900 ± 120	1	12,900 ± 190	1	S1?	Li et al. (2002)
ZK9											
	22.57	Plant material		7696 ± 26	7595 ± 25	8400 ± 10	1	8400 ± 25	1	S3	Wang et al. (2010)
	24.6			8012 ± 28	8010 ± 30	8810 ± 20	0.36	8890 ± 20	1	S3	Wang et al. (2010)
	28.5			8191 ± 48	8190 ± 50	9110 ± 35	0.43	9150 ± 135	1	S3	Wang et al. (2010)
	31.1			9171 ± 43	9170 ± 45	10,350 ± 35	0.52	10,335 ± 100	0.96	S2	Wang et al. (2010)
	36.7			9441 ± 37	9440 ± 35	10,680 ± 35	0.75	10,670 ± 90	1	S2	Wang et al. (2010)
	42.0			11,335 ± 56	11,335 ± 55	13,180 ± 60	1	13,180 ± 100	1	S1	Wang et al. (2010)
CM97											
Beta-117622	28.99	Molluscan shell	−7.5	8400 ± 50	8680 ± 50	9180 ± 100	1	9185 ± 180	1	S3	Hori et al. (2001a)
Beta-117623	40.20		−9.0	9740 ± 50	10,000 ± 50	10,800 ± 110	1	10,830 ± 200	1	S2	Hori et al. (2001a)
Beta-117624	61.06	Snail shell	−5.9	10,820 ± 50	11,140 ± 50	12,560 ± 65	1	12,530 ± 160	1	S1	Hori et al. (2001a)
JS98											
Beta-130646	34.60	Molluscan shell	−6.4	7220 ± 60	7530 ± 60	8360 ± 50	0.93	8310 ± 110	1	S3	Hori et al. (2001a)
Beta-130647	35.30		−5.9	7500 ± 60	7810 ± 60	8120 ± 90	1	8140 ± 160	1	S3	Hori et al. (2001a)
Beta-132939	36.55		−4.1	8200 ± 40	8540 ± 40	9010 ± 80	1	8990 ± 200	1	S3	Hori et al. (2001a)
Beta-130649	44.55		−8.5	9510 ± 90	9780 ± 90	11,200 ± 110	1	11,230 ± 170	0.82	S2	Hori et al. (2001a)
Beta-130650	45.46		−9.0	9780 ± 80	10,040 ± 80	11,560 ± 160	0.95	11,550 ± 280	0.96	S2	Hori et al. (2001a)
Beta-130652	52.56		−9.2	10,250 ± 100	10,510 ± 100	1,2500 ± 130	0.84	12,390 ± 290	1	S1	Hori et al. (2001a)
HQ98											
Beta-130658	28.6	Molluscan shell	−4.6	6830 ± 70	7170 ± 70	7520 ± 70	1	7530 ± 140	1	S3	Hori et al. (2001a)
Beta-130659	30.12	Plant material	−28.4	8130 ± 70	8080 ± 70	9050 ± 80	0.72	8930 ± 210	0.93	S3	Hori et al. (2001a)
Beta-130660	42.75	Plant material	−26.9	9080 ± 120	9050 ± 120	10,210 ± 90	0.59	10,145 ± 370	1	S2	Hori et al. (2001a)
Beta-130661	48.32	Molluscan shell	−10.3	10,250 ± 80	10,490 ± 80	11,410 ± 180	1	11,490 ± 320	1	S1	Hori et al. (2001a)
Beta-130664	55.50		−9.2	10,250 ± 70	10,510 ± 70	12,480 ± 100	0.96	12,440 ± 210	0.94	S1	Hori et al. (2001a)
Beta-132942	57.95		−10.2	10,240 ± 40	10,480 ± 40	12,460 ± 60	1	12,470 ± 90	0.84	S1	Hori et al. (2001a)
CJK11											
WHOI-101954	28.12	Foraminifera	0.05		4840 ± 35	4920 ± 75	1	4970 ± 160	1	Modern delta	Xu et al. (2016)
WHOI-101959	31.92	Foraminifera	−2.71		7010 ± 35	7380 ± 55	1	7380 ± 110	1	Modern delta	Xu et al. (2016)
CJK07											
WHOI-89060	0.19	Foraminifera	0.12		7250 ± 40	7600 ± 55	1	7585 ± 110	1	S3	Xu et al. (2016)
WHOI-101950	3.46	Foraminifera	−0.41		7320 ± 50	7640 ± 60	1	7665 ± 130	1	S3	Xu et al. (2016)
WHOI-101951	9.56	Foraminifera	−1.14		7580 ± 35	7900 ± 55	1	7900 ± 120	1	S3	Xu et al. (2016)

Note: In this paper, the 2 σ calibrated ages are adopted, and some are labeled in Figures 2, 3, and 11. Pro.—probability; S—succession; F—facies.
*Ages not used because they do not follow the general trend.

sparse bioturbation (BI 0–1; Table 2; Fig. 4C). Intervals dominated by OM2 layers are usually associated with coarse-grained sand and show an overall thinning-upward trend (F4a; for all references to facies, see later section on "Facies Analysis and Interpretation"; Table 2; Fig. 4D). Elsewhere, they occur sparsely in OM1-dominated intervals (F5b and F5c; Table 2; Fig. 4B), or they are locally present at the top or bottom of DM layers (F5b; Table 2; Fig. 4E). In these latter occurrences, the sandier-muddier cyclicity is not common.

Figure 3 (*on following page*). Columnar sections of the newly drilled cores ZK02 (A; landward core) and ZK01 (B; seaward core) from the modern Changjiang delta plain (see Fig. 1 for locations). Black circles indicate the depths at which various features were observed. SS—sedimentary structure; BF—benthic foraminifera; FS—flooding surface. S1, S2, and S3 represent successions 1, 2, and 3, respectively. All ¹⁴C ages are calibrated and reported in (cal.) k.y. B.P. (see more details in Table 1).
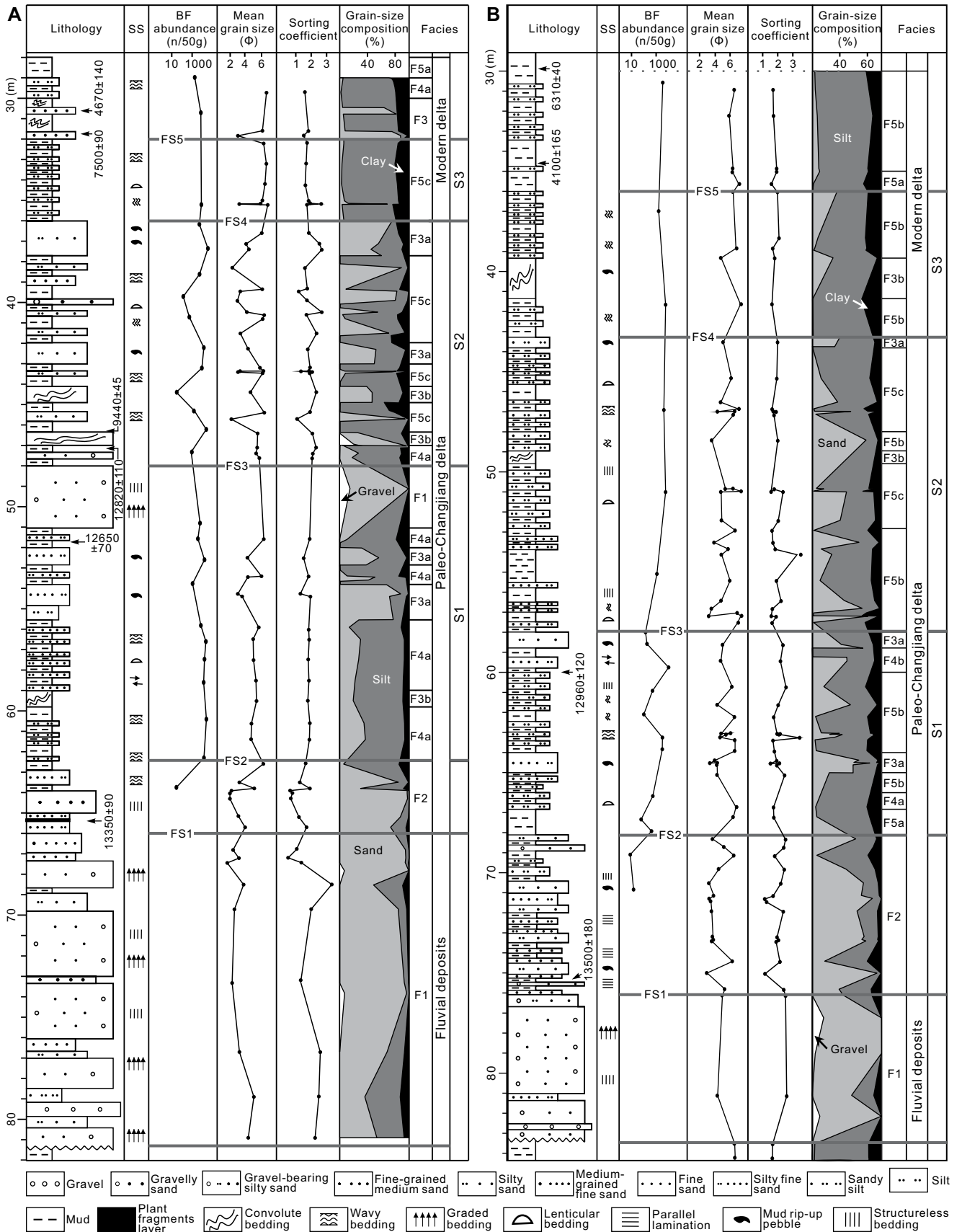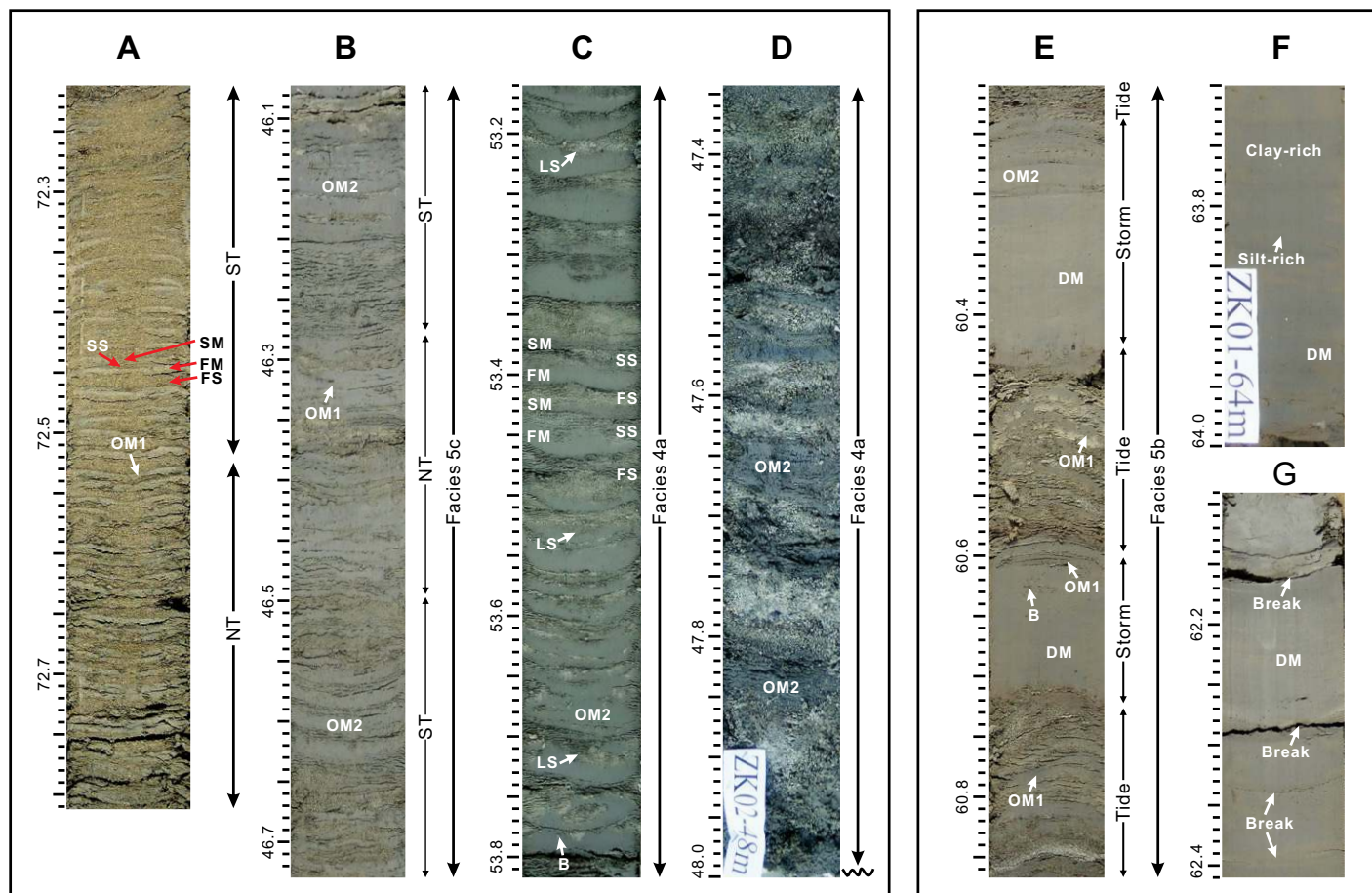
Figure 3.

Organized mud layers types 1 and 2 (OM1 and OM2)

Disorganized mud layers (DM)

Figure 4. Photographs of cores ZK01 and ZK02 showing typical features of the organized (OM1 and OM2) and disorganized (DM) mud-layer types (depth in m). (A) A group of OM1 mud layers (generally <1 cm thick) interlaminated with fine sand layers (72.20–72.80 m depth; core ZK01). On a small scale, this interval shows obvious thick-thin alternations in the thickness for both the sand and OM1 mud layers, more commonly for the sand layers, which is interpreted to represent the tidal diurnal inequality, with the thicker sand and mud layers (termed as the first sand [FS] and first mud [FM] layers) being deposited during the larger tides, and the thinner sand and mud layers (i.e., the second sand [SS] and second mud [SM] layers) being formed during the smaller tides. On a larger scale, the variation in the thickness of the sand layers shows an alternation of sandier and muddier intervals, which is interpreted to represent evidence of neap-spring cycles, with the sandier and muddier intervals formed during spring tides (ST) and neap tides (NT), respectively. (B) Examples of OM1 and OM2 mud layers (46.07–46.73 m depth; core ZK01). As with the interval in A, the OM1 layers and accompanying sandy and silty layers display pronounced sandier and muddier alternations, representing the neap-spring cycles. Note the thicker OM2 (generally >1 cm) layers interspersed in the OM1-dominated interval that occur preferentially in association with the coarsest and thickest sand layers. As a result, they are interpreted to have formed during spring tides. (C) Examples of OM2 mud layers interbedded with fine sand and coarse silt layers in F4a (53.15–53.80 m depth; core ZK02). They are thick (1–5 cm) and internally homogeneous, and they locally display prominent thick-thin layer-thickness alternations showing evidence of the tidal diurnal inequality. Sparse bioturbation (B) with bioturbation index (BI) of 0–1 and small load structures (LS) are present at the top of many OM2 layers. (D) The coexistence of thick, homogeneous OM2 mud layers and relatively coarse-grained sand layers in F4a (47.35–48.00 m depth; core ZK02), displaying a thinning-upward trend for the OM2 mud layers, indicating a decrease of suspended-sediment concentrations, which is interpreted to be due to the waning of a river flood. (E) Examples of DM mud layers, which are extremely thick (5–30 cm) and internally structureless (60.20–60.85 m depth; core ZK01). They are randomly dispersed among OM1-dominated, tidally generated heterolithic intervals, with gradational or abrupt upper and lower contacts. Bioturbation (B) is present only at the top of each layer. (F) DM mud layers containing horizontal layering characterized by the alternation of silt-rich and clay-rich layers, which are interpreted to reflect variations in wave energy (63.70–64.00 m depth; core ZK01). (G) DM layers containing pronounced breaks that are believed to represent erosion by more intense wave action during an otherwise continuous storm (62.10–62.40 m depth; core ZK01).

The DM style of layering generally consists of unusually thick (5–30 cm) and homogeneous mud layers that are randomly interbedded within the laminated sand and OM deposits (Table 2; Fig. 4E). The contacts with the over- and underlying deposits can be either sharp or gradational (Table 2; Fig. 4E). In the case of a gradational upper contact, the mud-layer type changes gradually from DM to OM2 (locally absent) and then to OM1, whereas gradational basal contacts show the reverse trend (Table 2; Fig. 4E). Internally, the DM layers locally show faint horizontal layering with alternations of more silt-rich and more clay-rich sediment (Table 2; Fig. 4F). Pronounced breaks, as distinct from the subtle textural changes, are common within DM layers (Table 2; Fig. 4G). Bioturbation is generally absent from the body of DM layers, but it is commonly present at the top (Table 2; Fig. 4E), with a BI of 0–1, and a few examples with a BI of 3.

These three types of mud layers are interpreted to have distinct origins (Table 2). The cyclic variation of sand-layer thicknesses in OM deposits implies that they were formed by the periodic variation in tidal-current strength; as a result, the OM layers are believed to have formed during tidal slack-water periods, when suspended sediment settled (Table 2). In particular, the thick-thin layering is interpreted as indicating the diurnal inequality, whereas the gradual variation from muddier to sandier intervals is believed to represent neap-spring cycles (Table 2). However, the neap-spring cyclicity is not always definitive, because the number of layers is rarely close to 28 (or 56; cf. Kirby and Parker, 1983; Dalrymple et al., 2003; Schrottke et al., 2006; Baas et al., 2009; Mackay and Dalrymple, 2011). By contrast, the DM layers are interpreted to be generated by waves based on their noncyclic distribution, their great thickness, and their occurrence in more distal settings (see more later herein; Table 2). Similar deposits have been reported from the inner shelf, offshore of the Amazon River (Jaeger and Nittrouer, 1995; Kuehl et al., 1996; Kineke et al., 1996), the Eel River continental shelf (Hill et al., 2007), the modern Fly River delta (Dalrymple et al., 2003), and the delta-front environments from the Jurassic Tilje Formation, offshore Norway (Ichaso and Dalrymple, 2009). They have also been found in the delta-front region of the modern Changjiang delta (Shen et al., 1992).

Based on the thickness of the various types of mud layers, the OM1 layers (<1 cm thick) represent classic slack-water mud drapes generated by normal gravitational settling of suspended sediments during short, tidal slack-water periods in locations or at times when suspended-sediment concentrations were less than 1 g/L (Table 2; cf. McCave, 1970; Ichaso and Dalrymple, 2009;

Mackay and Dalrymple, 2011). By contrast, OM2 and DM layers are interpreted to represent fluid-mud deposits (i.e., dense, bottom-hugging suspensions with suspended-sediment concentrations >10 g/L) because of their thickness (>1 cm) and texturally homogeneous nature, as well as the absence of bioturbation, except for limited postdepositional colonization (Table 2; cf. Dalrymple et al., 2003; Dalrymple and Choi, 2007; Ichaso and Dalrymple, 2009). High suspended-sediment concentrations within fluid-mud bodies hindered settling, which inhibited vertical segregation of materials with different settling velocities, resulting in the development of homogeneous mud layers that lack grading (Table 2; Kirby and Parker, 1983; Mackay and Dalrymple, 2011). The low bioturbation indices likely resulted from the elevated suspended-sediment concentrations and the soup-ground conditions, which inhibited substrate colonization (cf. MacEachern et al., 2010; Mackay and Dalrymple, 2011).

Fluid muds are most common and/or widespread in coastal and shelf environments during spring tides (Dalrymple et al., 2003; Ichaso and Dalrymple, 2009; Mackay and Dalrymple, 2011), river floods (Ichaso and Dalrymple, 2009; Wu et al., 2012), and storms (Jaeger and Nittrouer, 1995; Kuehl et al., 1996; Kineke et al., 1996), when suspended-sediment concentrations are highest due to the resuspension of previously deposited mud. Most occurrences of OM2 fluid-mud layers occur in Facies 4a (Figs. 4C and 4D; see additional description later herein), which consists of an alternation of OM2 mud layers and coarse-grained sand layers, and which shows a thinning-upward trend that is interpreted to correlate with river floods that were modulated by tidal currents (Table 2). The thinning-upward trend indicates the progressive decrease of suspended-sediment concentrations due to the waning of the river flood (Bhattacharya, 2010), as was the case in the Jurassic Tilje Formation, offshore Norway (Ichaso and Dalrymple, 2009, 2014). The OM2 layers occurring in association with OM1 layers exhibit cyclic sandier and muddier trends associated with neap-spring tidal rhythmites (Fig. 4B), and they are interpreted to represent the deposits formed during spring tides (Table 2). Such fluid-mud layers occur mainly within tidal channels (Dalrymple et al., 2003; Mackay and Dalrymple, 2011; Chen et al., 2015), but they are also present locally in the intertidal zone, as is the case in the open-coastal tidal flats in the modern Changjiang delta (Fan et al., 2004).

The DM type fluid-mud layers are attributed to storm-wave action that commonly persists for several days and generates very high suspended-sediment concentrations (Table 2; Xu et al.,

1990; Shen et al., 1992); as a result, they are usually much thicker than the mud layers formed during tidal slack-water periods. The subtle layering and pronounced breaks within them are thought to reflect variations in wave energy that caused pulses of erosion and deposition. The OM2 layers present at the bottom or top of DM layers may represent deposits generated by wave action modulated by tides during the initial waxing or final waning stages of storms (Table 2).

Facies Analysis and Interpretation

The late Pleistocene to early Holocene transgressive succession in cores ZK01 and ZK02 can be classified into five environmentally significant facies (generally 0.5–4.0 m thick for each facies occurrence, but locally reaching up to 15 m thick; Fig. 3; Table 3). The distinctions are based primarily on bulk grain size, as determined mainly by the relative proportion of sand and mud layers, the type and distribution of the mud layers, the vertical succession, gastropod and foraminifera content, and the degree of bioturbation or rooting.

Facies 1 (F1): Coarser-Grained Structureless Sand (Amalgamated Fluvial Channel)

Units of F1 (3–13 m thick) are erosionally based and consist of several superimposed fining-upward successions (each ~0.5–3.0 m thick), with the sediments changing upward from gravelly sand or sandy gravel to fine or medium sand within each succession (Fig. 5A; see more details in Table 3). The gravel clasts are of extrabasinal origin, with diameters generally in a range of 2–50 mm. Sparse (up to ~10%) mud rip-up pebbles with dimensions larger than the core diameter (Fig. 5A), pieces of wood, and reddish-brown oxide stains are scattered throughout F1. Crude unidirectional cross-bedding and parallel lamination occur locally; contorted bedding (i.e., slump structures) is present but is not common. Tide-influenced sedimentary structures and foraminiferal fossils are absent, except within the mud rip-up pebbles. Some intact gastropod fossils occur locally, characterized by *Gyraulus* sp., *Tulotomoides* sp., and *Gyraulus cf. Planoconcavus* Gu, 1989, all of which live in freshwater (cf. Yu et al., 1963; Gu and Wang, 1989; Zhao, 1992). Bioturbation is absent (BI 0), as are mud layers.

The presence of a basal-erosional surface, a general upward-fining succession beginning with gravel, unidirectional cross-bedding, and reddish-brown oxide stains indicates that F1 was deposited in a channel-thalweg to basal point-bar setting in a river (Table 3; cf. Nittrouer et al., 2011). The repetitive erosive-bounding surfaces and stacked nature of these channel

successions (Fig. 5A) indicate repeated channel migration or avulsion and reoccupation (Table 3; cf. Goodbred and Kuehl, 2000a). The absence of foraminifera and tidal lamination, and the presence of freshwater gastropod fossils imply that F1 represents amalgamated fluvial-channel sediments deposited upstream of the tidal and saltwater limits (cf. Pemberton et al., 1992; Zhang et al., 2014).

Facies 2 (F2): Alternation of Coarser-Grained Structureless Sand and Heterolithic Stratification (Tide-Influenced Fluvial Channel)

Facies 2 is 3–8 m thick and is characterized by the repetitive alternation of structureless sand beds and intervals of laminated heterolithic stratification (Table 3). The structureless sand beds (generally 0.1–1.5 m thick) are erosively based and are mainly composed of silty sand and silty fine sand with minor amounts of gravel-bearing coarse sand (Fig. 5B; see more details in Table 3). Irregular mud rip-up pebbles, intact gastropod fossils (dominated by freshwater genus *Tulotomoides* sp.; cf. Yu et al., 1963; Zhao, 1992), crude parallel lamination, and unidirectional cross-bedding occur sporadically (Fig. 5B); tidal sedimentary structures and marine fossils are absent (Table 3). The heterolithic intervals are generally 0.3–1.0 m thick, and they are characterized by the cyclic alternation of fine sand or sandy silt layers (2–20 mm thick; 30%–70% by volume) and OM1 layers (2–8 mm thick), which show rhythmic thick-thin alternations of successive sand layers and cyclic alternations of sandier and muddier intervals (Table 3; Fig. 5B). Terrestrial organic material is abundant within the heterolithic stratification locally (Fig. 5B). Benthic foraminifera (BF) dominated by *Ammonia beccarii* vars. were encountered sporadically in the heterolithic intervals, but bioturbation was not present.

The presence of an erosive-basal surface, coarser-grained sand, unidirectional cross-bedding, and freshwater gastropod fossils, and the absence of tidal structures and marine fossils suggest that the structureless sands in F2 accumulated in a channel that was dominated by freshwater fluvial currents (Table 3; cf. van den Berg et al., 2007; Dalrymple et al., 2015; Jablonski and Dalrymple, 2016). Conversely, the occurrence of double mud drapes, evidence of diurnal inequality (i.e., thick-thin alternations) and neap-spring rhythmic lamination (i.e., alternation of sandier-muddier intervals), and presence of scarce benthic foraminifera within the heterolithic intervals indicate that tidal currents were present and were more intense than fluvial currents at these times (Table 3). The alternation of periods of river and tidal dominance is interpreted to represent the record of river floods interspersed with interflood periods when tidal processes dominated (Table 3; cf. Dalrymple and Choi, 2007; van den Berg et al., 2007; Dalrymple et al., 2015; Jablonski and Dalrymple, 2016). Based on the scarce bioturbation, sporadic presence of foraminifera and freshwater gastropod fossils, thinness of mud layers (typically <5 mm), and local enrichment in terrestrial organic material, we suggest that F2 represents the deposits of tidally influenced fluvial channels that were located landward of the turbidity maximum zone, in a zone where suspended-sediment concentrations were low and the salinity of the water was fresh during river floods and only slightly brackish during interflood periods (Table 3; cf. Dalrymple and Choi, 2007). This facies is probably equivalent to the "tidal river" deposits reported by Hori et al. (2001a) and Xu et al. (2016) from this stratigraphic unit, and the tidally influenced fluvial-channel deposits in the modern Gironde estuary (Allen and Posamentier, 1993) and Late Cretaceous Middle McMurray Formation, northeastern Alberta, Canada (Dalrymple et al., 2015; Jablonski and Dalrymple, 2016).

Facies 3 (F3): Finer-Grained Structureless Sand and/or Contorted Deposits (Tidal-Channel-Floor Deposits)

Facies 3 is of relatively limited extent, with thicknesses generally <l–2 m, and it has erosive contacts with the under- and overlying deposits (Table 3; Fig. 6A). It can be divided into two main types: finer-grained structureless sands (F3a) and contorted muddy or sandy deposits (F3b; Table 3; Fig. 6A). Sand layers of F3a are mainly composed of well-sorted fine and very fine sand, with lesser amounts of medium and coarse sand (Table 3; Fig. 6A), making them finer than those of F1 and F2. Mud rip-up pebbles are common (diameters typically 0.5–4.0 cm; content 10%–30%), especially immediately above the erosional basal surface, with the abundance and size decreasing upward through an interval of ~0.5–1.0 m (Table 3; Fig. 6A). Large-scale cross-beds occur sporadically in the lower part (e.g., 58.65–58.80 m depth in Fig. 6A). F3b is usually <1 m thick with a sand-layer content of 0%–80% (Table 3; Fig. 6A). Within F3b, the mud and sand layers are intermixed, such that it is difficult to see the original sedimentary stratification (e.g., 46.35–47.00 m depth in Fig. 6A; Table 3). Sporadically, the sediments are characterized by contorted bedding (Table 3). In some occurrences, the deformed mud layers are >1 cm thick, indicating the original presence of fluid-mud deposits (OM2; e.g., 30.25–30.47 m depth in Fig. 6A). Foraminiferal fossils are abundant and diverse (Fig. 3; Table 3), and they are mainly composed of benthic foraminifera (27–37 species per 50 g dry sample), consisting principally of *Ammonia beccarii* vars., *Epistominella naraensis*, *Elphidium magellanicum*, *Cribrononion vitreum*, *Quinqueloculina* sp., and *Elphidium advenum*. In addition, this facies contains some heavily abraded bivalves. Bioturbation is not present.

Figure 5 (*on following page*). Core photographs showing the sedimentary characteristics of (A) amalgamated fluvial-channel (F1) and (B) tide-influenced fluvial-channel deposits (F2; depths in m). [Note: Straight vertical indentations and horizontal striations on the sediment surface are an artifact of cleaning the soft sediment surface or of shrinkage during drying. The aluminum spacers (light gray) indicate the locations of permeability samples.] OM1, OM2—organized mud layers. (A) Fluvial-channel deposits of F1 (48.00–51.11 m depth; core ZK02) resting erosionally on distal tidal-channel deposits (F4a; 51.11–52.00 m depth). F1 consists of structureless coarse-grained sand and contains four superimposed fining-upward successions (separated by subtle erosional breaks at 48.53 m, 49.27 m, and 50.20 m depth), with the sediments changing upward from gravelly sand or sandy gravel to fine or medium sand. Sparse mud rip-up pebbles (MRP, 48.87–49.20 m and 50.69–50.75 m depth), the nature of which reflects the character of the underlying heterolithic deposits, are present immediately over the erosional bases. (B) Tide-influenced fluvial deposits of F2 (72.00–76.00 m depth; core ZK01) characterized by the alternation of structureless sand (river-flood deposits) and heterolithic tidal stratification (interflood deposition), indicating the fluctuation of the dominant physical processes in response to variations in river discharge. The river-flood deposits are erosionally based and contain coarser sediments. The erosional base is inferred by the abrupt change in grain size (73.63 m and 75.74 m depth) and the presence of mud rip-up pebbles (MRP; 75.37 m depth). Crude parallel lamination (CPL; 75.52–75.60 m depth) and cross-bedding (CB; 73.37–73.45 m depth) are present sporadically. The interflood sediments are finer grained and heterolithic, and they are characterized by the alternation of fine sand and OM1 layers, which locally show tidal rhythmites containing neap-spring cycles (i.e., alternation of sandier and muddier intervals; 72.20–72.80 m depth) and evidence of diurnal inequality (thick-thin layer-thickness alternations; 72.40–72.50 m depth). For explanations of FS, SS, FM, SM, NT, and ST, see details in Figure 4A.
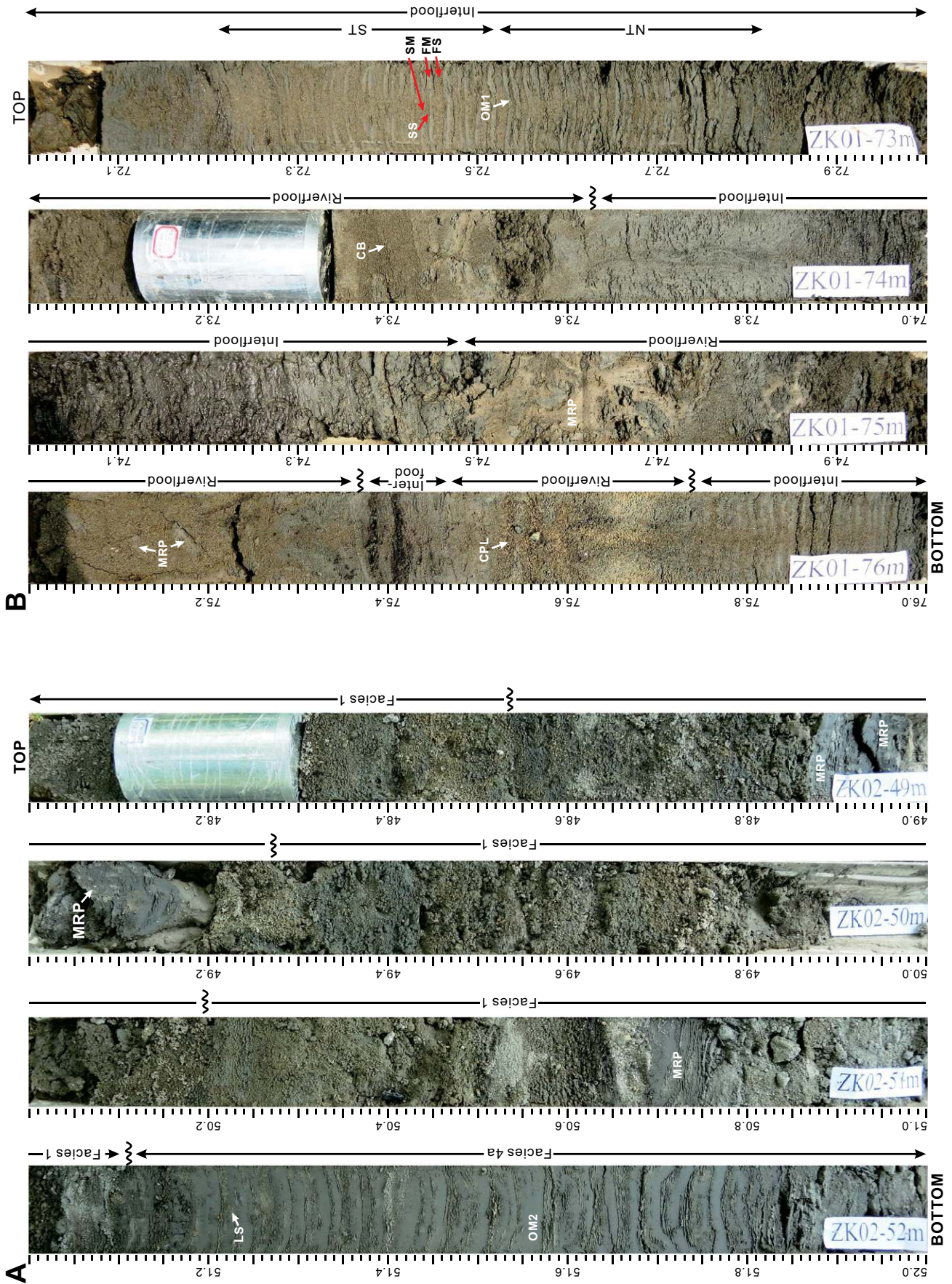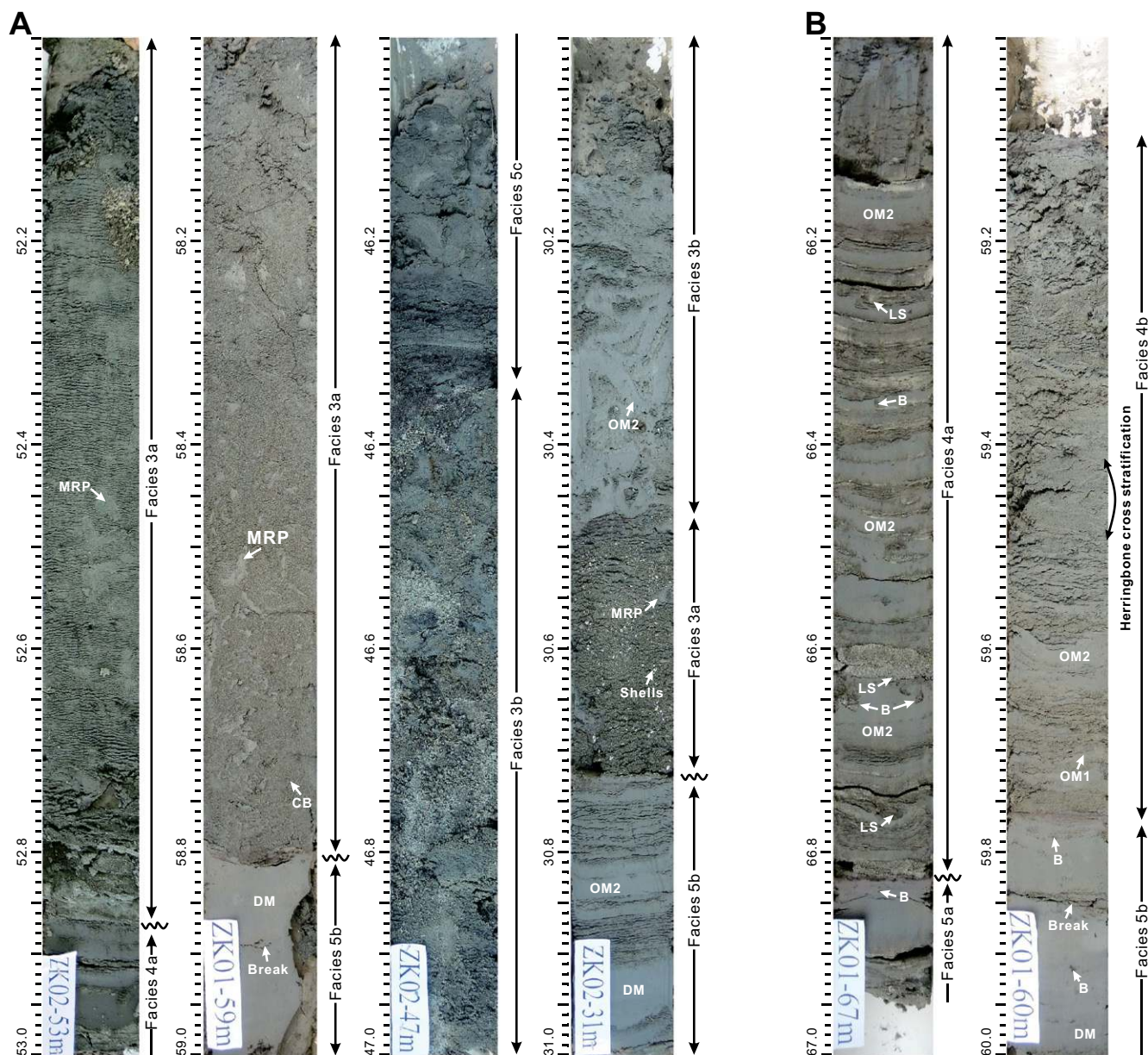
Figure 5.

Figure 6. Core photographs showing the sedimentary characteristics of tidal-channel-floor deposits (F3 and F4; depths in m). [Note: Horizontal striations are an artifact of cleaning the soft sediment surface or of shrinkage during drying.] OM1, OM2—organized mud layers types 1 and 2; DM—disorganized mud layers. (A) Examples of F3 in four different core intervals. Two main subfacies are present. F3a occurs as erosively based, finer-grained structureless sand with abundant broken shells (30.47–30.73 m depth in core ZK02), and mud rip-up pebbles (MRP; 52.00–52.86 m depth in core ZK02; 58.00–58.81 m depth in core ZK01). These MRPs are irregular and show an obvious decreasing-upward trend for both grain size and abundance. Crude cross-bedding (CB) occurs in the channel bottom (e.g., 58.65–58.80 m depth in core ZK01). F3b is typified by sharp-based, contorted deposits due to slumping from adjacent channel banks (e.g., 46.35–47.00 m and 30.00–30.47m depth in core ZK02), resulting in difficulty in recognizing original sedimentary structures and layering. Locally, the deformed mud layers are >1 cm thick, indicating the original presence of fluid-mud deposits. (B) Examples of F4 from two intervals of core ZK01. Two varieties are present. F4a (66.00–67.00 m depth) is characterized by the alternation of thick and homogeneous OM2 layers and coarse-grained sand layers, which show a thinning-upward trend for the OM2 mud layers, indicating a decrease of suspended-sediment concentrations, and a thinning- and fining-upward trend for sand layers, implying a decrease of current speed, generating a net, coarsening-upward trend, which is interpreted to be due to the waning of a river flood within the channel. Bioturbation (B) is scarce to absent, and some small load structures (LS) are present at the bottom of sand layers. F4b is interpreted to represent the toeset deposits of a dune within the terminal distributary channel, and it shows a coarsening- and sandier-upward trend. The bottom part of this succession consists of thinly to thickly laminated sandy silt and OM1 (with a few OM2 layers); the middle part is mainly composed of fine and very fine sand, and very coarse silt; and the top consists of medium and fine sand. Crude cross-bedding is abundant in the sand-dominated middle and upper parts, with evidence for current reversals (i.e., herringbone cross-stratification at 59.40–59.50 m depth).

The erosional basal surface, the presence of cross-bedding, the upward decrease in the abundance and grain size of mud rip-up pebbles, and meter-scale contorted bedding suggest a channel-base origin for F3 (Table 3). Contorted bedding is common in channel deposits and reflects the collapse of unstable banks (cf. Dalrymple et al., 2003; Choi et al., 2004; Legler et al., 2013; Chen et al., 2015). The ubiquitous presence of benthic foraminifera, which is marked by the coexistence of euryhaline (e.g., *Ammonia beccarii* vars.) and stenohaline types (such as *Epistominella naraensis* and *Quinqueloculina* sp.), implies the presence of a brackish-water environment, a condition similar to the setting in the (terminal) distributary channels of the modern Changjiang delta (Table 3; Li and Wang, 1998). As a result, F3 is interpreted as tidal-channel-floor deposits that accumulated in a relatively distal environment.

Facies 4 (F4): Bedded/Laminated Heterolithic Stratification (Tidal-Channel-Floor Deposits)

Units of F4 are generally <1 m thick, pervasively heterolithic, and erosively based, comprising two main types: fining- and thinning-upward heterolithic stratification (F4a), and coarsening- and thickening-upward heterolithics (F4b; Table 3; Fig. 6B). F4a is characterized by the alternation of sand or sandy silt and OM2 layers, and it commonly displays a thinning-upward trend for both the sand and mud layers, but the mud-layer thickness decreases more rapidly, generating an overall sandier-upward succession (Table 3; Fig. 6B). Sand, which constitutes <50% and usually only 30% of F4a, has a wide range of grain sizes, from coarse sand to silt, sporadically with granules, and generally occurs as thick laminae (usually <1 cm thick), but can locally be present as thick beds (1–15 cm thick), with the grain size decreasing upward through successive layers (Table 3; Fig. 6B). Internal structures are generally invisible. However, asymmetric ripples are pervasive as form sets on the top of sand layers, with symmetrical ripples occurring less commonly, implying the presence of current-ripple cross-lamination, sporadically influenced by waves (Table 3). Small-scale load structures are present at the base of many sand layers (Fig. 6B). Foraminiferal fossils are also abundant in F4a and are mainly composed of benthic foraminifera (28–42 species per 50 g dry sample), dominated by *Ammonia beccarii* vars., *Elphidium magellanicum*, *Epistominella naraensis*, *Cribrononion vitreum*, *Elphidium nakanokawaense*, *Florilus decorus*, *Protelphidium tuberculatum*, *Elphidium advenum*, and *Nonionellina atlantica* (Table 3; Fig. 3). Scarce bioturbation is commonly present at the top of OM2 layers with a BI of 0–1 (Fig. 6B).

F4b only occurs in core ZK01 (59.1–59.76 m depth) and consists of a coarsening- and sandier-upward succession (Table 3; Fig. 6B). Its lower part is characterized by thinly to thickly laminated sandy silt and OM1 layers, with a few OM2 layers (Fig. 6B). The middle part consists primarily of silty fine sand with a few mud drapes (OM1 layers) and herringbone cross-stratification (Fig. 6B). The top part comprises structureless to chaotic medium and fine sand deposits, which are probably due to disturbance by coring (Fig. 6B). Bioturbation is scarce with a BI of 0–1.

The presence of an erosional base and abundant, thick fluid-mud (OM2) layers in association with coarse-grained sand indicates that F4a represents tidal-channel-floor deposits accumulated beneath the turbidity maximum zone (Table 3), similar to those reported from the tidal-fluvial transition zone of many estuaries (e.g., Kirby and Parker, 1983) and deltas (e.g., Dalrymple et al., 2003; Ichaso and Dalrymple, 2009). The upward thinning of fluid-mud layers and upward-sandier nature of F4a reflect an upward decrease of suspended-sediment concentrations, whereas the upward thinning and fining of sand layers indicate the progressive decrease of current speed upward within the channel (Table 3; cf. Dalrymple et al., 2003; Ichaso and Dalrymple, 2014; Ichaso et al., 2016). As with F3, the ubiquitous presence of benthic foraminifera and the coexistence of euryhaline (e.g., *Ammonia beccarii* vars.) and stenohaline types (such as *Epistominella naraensis* and *Nonionellina atlantica*) further testify to the environmental interpretation (Table 3; cf. Li and Wang, 1998).

As for F4b, the presence of sand-mud couplets (i.e., tidal rhythmites) that include fluid-mud (OM2) layers, herringbone cross-stratification, and a coarsening- or sandier-upward succession indicates that it can be interpreted as the deposits of a compound dune on the bottom of a tidal channel (Table 3; cf. Dalrymple, 2010; Olariu et al., 2012), a situation that exists in the tidal channels throughout the modern Changjiang delta, including the area beneath the turbidity maximum zone (Zhou, 1983; Cheng et al., 2004; Li et al., 2005; Li et al., 2008; Wu et al., 2009; Wu et al., 2016). The dunes that occur beneath the turbidity maximum zone of the modern Changjiang delta show a wide range of heights (0.13–1.84 m), which is consistent with the thickness of the F4b succession in core ZK01.

Facies 5 (F5): Alternation of Laminated Heterolithic Stratification and DM Layers (Tidal-Bar or Distal Muddy Deposits at the Mouth of a Tide-Dominated System)

Facies 5 shows an alternation of two types of deposits (Table 3; Fig. 7). The first consists of laminated to bedded sand or silt (layers 1–35 mm thick; content 30%–80%) separated by OM1 mud layers (dominant) with a subordinate number of OM2 layers (Table 3; Fig. 7). Sporadically, quasiregular alternations of muddier and sandier intervals are present (Table 3; Fig. 7). Wavy, lenticular, and flaser bedding are common, with pervasive current-ripple cross-lamination in the sand layers (Table 3). DM layers with thicknesses of 5–30 cm are randomly interspersed within these heterolithic deposits (Table 3; Fig. 7). The thickness of the DM layers is significantly greater than the mud layers in the heterolithic deposits, and the degree of bioturbation is overall lower (BI 0–1), with the bioturbation occurring only at the top of each DM layer (Tables 2 and 3; Figs. 4E and 7). F5 can be further divided into three subfacies (Table 3). F5a is composed mainly of DM layers (>70% by volume), and F5b is typified by 30%–50% DM layers (Fig. 7). No obvious vertical trend of DM abundance is observed within these subfacies. F5c generally contains less than 10% DM layers, and the mud-layer thickness usually decreases upward (Fig. 7). Bioturbation is relatively more abundant in F5c, with a BI of 1–3 (average BI 2), whereas the BI of F5a and F5b is generally 0–1 (Table 3). Foraminifera fossils, dominated by benthic foraminifera, are also abundant in F5 (13–44 species per 50 g dry sample), and are characterized by *Ammonia beccarii* vars., *Epistominella naraensis*, *Florilus decorus*, *Elphidium magellanicum*, *Quinqueloculina* sp., *Cribrononion vitreum*, *Nonionellina atlantica*, and *Nonionella jacksonensis* (Table 3; Fig. 3). In general, the average proportion of *Ammonia beccarii* vars. decreases from 31% in F5b and F5c to 23% for F5a, and the content of deep-water species (such as *Epistominella naraensis*, *Quinqueloculina* sp., *Nonionellina atlantica*, and *Nonionella jacksonensis*; water depth generally >30 m; cf. Li and Wang, 1998; Wang et al., 2014) has an inverse tendency (Table 3).

Based on the interbedding of OM and DM layers, we interpret this facies to reflect an alternation between times of tide domination (laminated heterolithics containing OM1 and OM2 layers) and wave domination (the DM layers, which represent storm deposits; Tables 2 and 3). In tide-dominated systems, the thickness and abundance of DM layers should decrease landward because of the landward decrease in wave energy due to friction (Dalrymple and Choi, 2007), and also upward in channels because the mud resuspended by waves tends to flow downslope (cf. Traykovski et al., 2000), where it would accumulate preferentially in the bottom of channels. Thus, F5a can be interpreted as sediments formed in the mouth of the system where wave action was episodically intense, yet tidal currents dominated sedimentation during

the periods between storms. This environmental interpretation is confirmed by the relatively higher content of deep-water foraminiferal fossils and lower abundance of *Ammonia beccarii* vars., relative to F5b and F5c, an assemblage that is similar to that found in the prodeltaic to shallow-marine environment of the modern Changjiang delta (cf. Li and Wang, 1998; Li et al., 2014). Facies F5b and F5c are interpreted to represent tidal-bar deposits adjacent to the tidal channels, at higher elevations that were not as favorable for the accumulation of abundant fluid-mud deposits. F5b, with its greater abundance of DM layers, is interpreted to have formed at locations more seaward and/or deeper than F5c, and it is similar to the deposits that have been documented from the distal delta-front area in the Fly River delta (e.g., facies 9 *in* Dalrymple et al., 2003). Indeed, the sedimentary characteristics and foraminiferal assemblage of F5a and F5b are identical to those of the distal delta-front and prodeltaic deposits of the modern Changjiang delta recovered in core ZK02 (Fig. 8), and in surface samples from similar present-day environments (Wang et al., 2005).

In summary, the sandy deposits in the various facies show a seaward-fining trend from coarse sand and gravel in the amalgamated fluvial-channel deposits of F1, through medium and fine sand in the tide-influenced fluvial channels (F2), to fine or very fine sand and silt in the tidal channels (F3 and F4), and finally to mud-dominated deposits that characterize the mouth of the system (F5a; Figs. 9A, 9B, and 9C). With regard to the muddy deposits, the mud-layer type and thickness display several significant variations between the facies (Figs. 9A, 9B, and 9C): (1) Mud layers are absent from the purely fluvial deposits of F1; (2) the tidal-fluvial channels (F2) are dominated by thin OM1 layers; (3) thick OM2 fluid-mud layers first appear in channel-bottom deposits from the inner part of the tidal-fluvial transition (e.g., F4a in succession 2 of core ZK02; Fig. 4D) and become progressively more abundant in a seaward direction (e.g., F4a in succession 1 from core ZK01; Fig. 7); and (4) randomly disposed, anomalously thick, storm-generated DM fluid-mud layers are abundant in the muddy deposits that accumulated at the mouth of the system. With regard to the fossils present, freshwater gastropod fossils occur only in fluvial deposits (F1 and F2) and are absent in distal tide-dominated deposits (F3, F4, and F5); the abundance of *Ammonia beccarii* vars., a species that inhabits low-salinity water, decreases seaward, whereas the content of deep-water (>30 m depth) and stenohaline benthic foraminifera is highest in F5a, the most distal facies.

Facies Successions

Based on the facies described here, it is evident that the unit of interest (i.e., the late Pleistocene to early Holocene transgressive deposits in cores ZK01 and ZK02) begins with fluvial sands and gravels (F1), followed upward by somewhat finer-grained, tidal-fluvial channel deposits (F2). These are then overlain by a succession of much more muddy, pervasively heterolithic deposits that accumulated in a range of tidal-channel-bottom (F3 and F4) and flanking, tidal-bar environments (F5b and F5c), with interspersed intervals of distal muddy deposits (F5a; Figs. 3 and 5–7). This transgressive succession is overlain by the upward-sanding tidal deposits of the modern delta (Fig. 3). The transgressive-aged tidal deposits can be subdivided into three smaller-scale upward-sanding successions (successions 1, 2, and 3), in which the depositional environment became progressively more proximal and shallow upward in each succession (Figs. 3 and 10). Based on the available ^{14}C dates, the various depositional units identified are temporally correlative between the ZK01 and ZK02 cores (Figs. 3 and 11; Table 1). The following analysis is based on this interpretation.

Succession 1 is ~14 m thick in the landward ZK02 core and ~10 m thick in the seaward ZK01 core. In core ZK02, it overlies F2 (tide-influenced fluvial-channel deposits) abruptly and is composed of a succession of tidal-channel deposits (F3 and F4a), the top of which is incised by purely fluvial channel deposits (F1; Fig. 3A). The abrupt increase in the abundance of foraminifera at the base of succession 1 in core ZK02 confirms the sudden deepening and flooding (i.e., the abrupt transition from F2 to F4a; Fig. 10). This is followed, however, by an upward decrease in the abundance of planktonic and benthic foraminifera, the number of benthic foraminifera species, and the contents of some typical foraminifera such as *Epistominella naraensis* and *Cribrononion vitreum*, which are all consistent with the shallowing-upward trend inferred from the sedimentary facies (Fig. 10). In core ZK01, the lower part of succession 1 consists of wave-influenced distal muddy deposits (F5a; dominated by DM layers; Figs. 3B and 7), which abruptly overlie the proximal fluvial-dominated channel deposits of F2 at the top of the underlying succession. Upward, the deposits change gradually into sandier tidal-bar deposits (F5b), and then they are truncated by muddy or sandy tidal-channel-floor deposits that lack evidence of wave action (F3a and F4; Figs. 3B and 7). This succession of facies clearly indicates an upward-shallowing trend with more landward facies overlying more distal facies.

Succession 2 is ~12 m thick in the landward ZK02 core and ~14 m thick in the seaward ZK01 core. In core ZK02, tidal-channel deposits (F4a) rest abruptly on purely fluvial channel deposits (F1), whereas in core ZK01, wave-influenced tidal-bar sediments (F5b) suddenly overlie sandy tidal-channel deposits (F3a) of succession 1 (Fig. 3). Succession 2 is characterized by the alternation of sandy and muddy channel-bottom (F3 or F4a) and muddy tidal-bar deposits (F5b and F5c; Fig. 3). In core ZK02, the sudden increase of foraminiferal fossils at the base of succession 2 also indicates a clear shift to a more distal environment,

---

Figure 7 (*on following page*). Photographs of selected intervals of core ZK01 showing the sedimentary characteristics of prodelta and tidal-bar deposits in the delta front (F5; depth in m). Also depicted are the features of organized (OM1 and OM2) and disorganized (DM) mud layers. [Note: Horizontal striations are an artifact of cleaning the soft sediment surface or of shrinkage during drying. The aluminum spacers (light gray) indicate the locations of permeability samples.] F5 is characterized by the alternation of laminated heterolithic deposits and DM layers. The former consist primarily of thinly to thickly laminated sand and OM1 layers (<1 cm thick). F5 consists of three main types. F5a (66.82–68.00 m depth) is dominated by DM layers (>70% by volume), indicating the presence of episodic intense wave action; this subfacies is interpreted as prodeltaic deposits. F5b (60.00–63.00 m depth) and F5c (45.00–47.00 m depth) are interpreted as tidal-bar deposits, with content of DM layers of 30%–70% and <30%, respectively, which are then truncated by terminal-distributary-channel deposits (i.e., F3a at 64.00–65.00 m depth). F5b, with its greater abundance of DM layers, is interpreted to have formed more seaward and/or deeper than F5c. The vertical trend for mud layers is not obvious in F5b, while it is present in F5c. F5c locally shows a larger-scale variation in sand- and mud-layer thickness (e.g., at 46.08–46.70 m depth) that is attributed to neap-spring cycles. Note the overall upward thinning of mud layers and the upward increase of bioturbation (B), with the bioturbation index (BI) increasing upward from 0–1 to 1–3. In these deposits, the OM2 fluid-mud layers are preferentially present in the spring-tide (ST) intervals. See abbreviations in Figure 4.
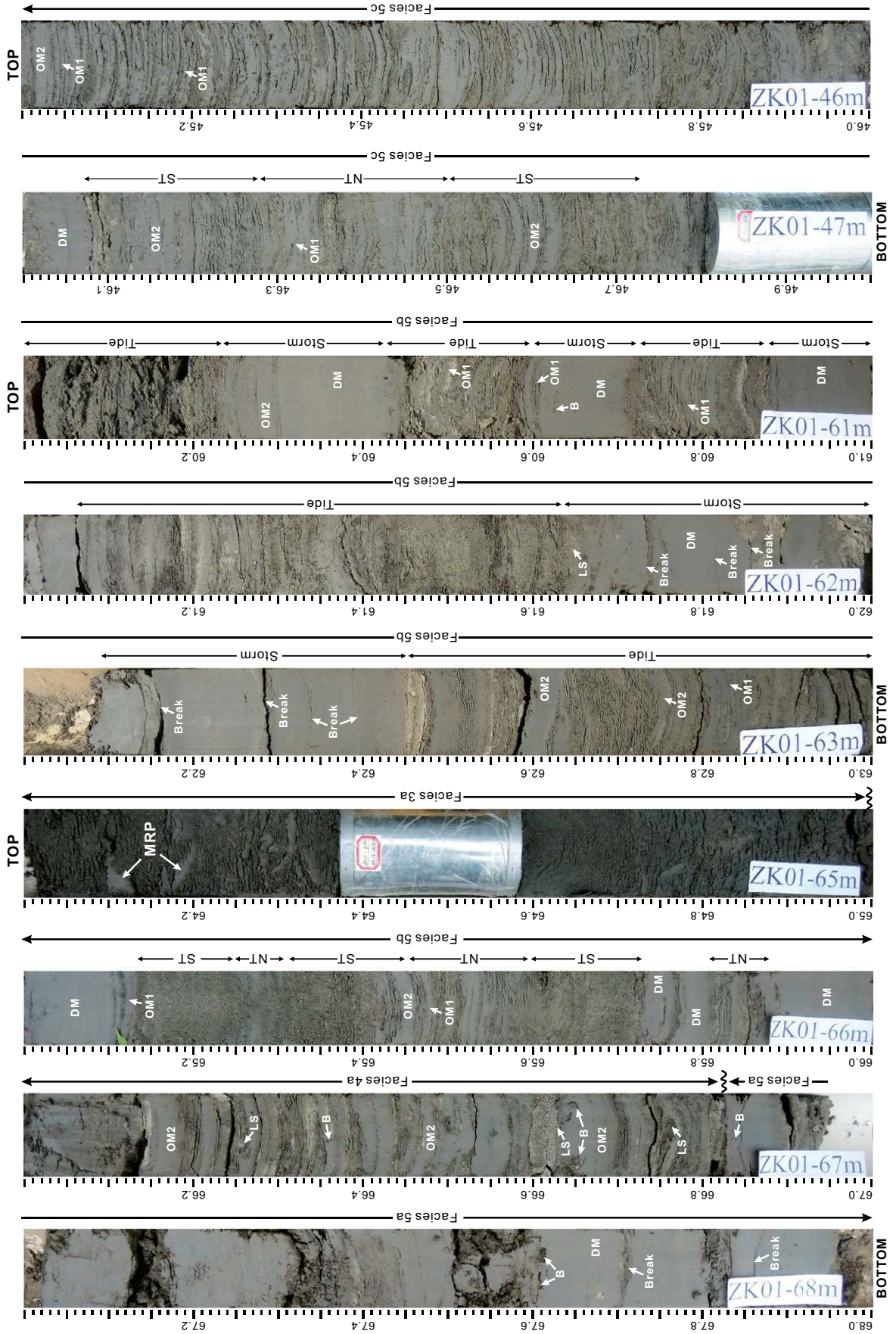
Figure 7.

TABLE 2. CHARACTERISTICS OF THE TWO MUD-LAYER TYPES DISTINGUISHED IN THIS STUDY

Mud-layer subfacies	Mud-layer thickness	Internal structures of mud layers	Nature of upper and lower contacts of mud layers and vertical succession	Sand/silt layers between successive mud layers	Origin of mud layers
OM (organized mud): presence of tidal rhythmicity					
OM1	<1 cm, typically 2–5 mm	Texturally homogeneous. Weakly to moderately bioturbated (BI 0–3).	Sharp or gradational upper and lower contacts. Commonly occurs interlaminated with sand or coarse silt, the layers of which show regular variations in thickness, generating cyclic thick-thin layers, and locally gradational alternations between sandier and muddier intervals.	Comprising ~30%–80% by volume within OM1-dominated intervals. Grain size of sand layers has a wide range, including silt, sandy silt, and fine sand. Layer thickness ranges from 1 mm to 35 mm.	Tide-generated classic mud drapes: normal gravitational settling of suspended sediments during slack-water periods in settings with SSCs <1 g/L, such as during periods between river floods or during neap tides in the areas beneath the TMZ, or at any time in areas outside the TMZ.
OM2	1–5 cm	Lithologically structureless. Sparse bioturbation (BI 0–1) present at the top of mud layers.	Sharp upper and lower contacts. Usually associated with coarse-grained sand and showing an overall thinning- and sandier-upward trend, without significant sandier-muddier cyclicity. Dominant mud-layer type in some intervals; also occurs sparsely in OM1-dominated intervals. Some small load structures present on the top of mud layers.	Sand, which constitutes <50% and usually only 30% of the OM2-dominated intervals, has a wide range of grain size, from coarse sand to silt, sporadically with granules, and generally occurs as thick laminae (usually <1 cm thick), but locally can be present as beds with thicknesses reaching up to 15 cm.	Tide-generated fluid mud, based on their homogeneous nature, thickness (>1 cm), and near absence of bioturbation: hindered settling of suspended sediment during slack-water periods in areas with high SSCs (>10 g/L). OM2-dominated intervals associated with coarse sand and showing a thinning- and sandier-upward trend are interpreted to represent river floods that were modulated by tidal currents. Uncommon OM2 layers in OM1-dominated intervals were formed during spring-tide periods.
DM (disorganized mud): noncyclic distribution					
	5–30 cm	Generally homogeneous but locally shows faint horizontal layering with alternations of more silt-rich and more clay-rich sediment. Pronounced breaks are common within individual layers. Bioturbation is nearly absent (BI 0–1), except for postdepositional colonization.	Sharp or gradational upper and lower contacts. The mud-layer type can change gradually from DM to OM2 (locally absent) and then to OM1, where the upper contact is gradational, or vice versa in cases with a gradational lower contact. In general, DM layers are randomly interbedded with tide-generated heterolithic stratification.	Sand layers in the tide-generated heterolithic stratification interbedded with DM layers similar to those in the OM1-dominated intervals.	Wave-generated fluid mud as indicated by their homogeneous nature, great thickness (>5 cm), and near absence of bioturbation: hindered settling of suspended sediment during periods of strong wave action that persisted for several days or weeks, generating extremely high SSCs (>10 g/L). The subtle layering and pronounced breaks reflect variations in wave energy that caused pulses of erosion and deposition. The OM layers present at the bottom or top of DM layers may represent deposits generated by wave action modulated by tides during the initial waxing or final waning stages of storms.

Note: BI—bioturbation index; SSCs—suspended-sediment concentrations; TMZ—turbidity maximum zone.

whereas the shallowing-upward trend that is seen in succession 1 is not as obvious in succession 2, perhaps because of the sparse samples, lithological influence, or the existence of a more aggradational rather than progradational character (Fig. 10).

Succession 3 is ~4 m thick in core ZK02 and ~7 m thick in core ZK01. It abruptly overlies the underlying succession 2, with distal muddy tidal-bar deposits (F5b and F5c; wave-generated DM layers are present in the seaward ZK01 core) resting on more proximal sandy tidal-channel deposits (F3a), and it consists of an alternation of contorted channel-floor deposits (F3b) and heterolithic channel-bank deposits (F5b and F5c; Fig. 3). The top of succession 3 is abruptly overlain by wave-influenced, tide-dominated prodeltaic muddy deposits (F5a) of the modern Changjiang delta in core ZK01, and it is separated by classic transgressive lag deposits consisting of relatively well-sorted fine sand and abundant broken shells (F3a) in the landward ZK02 core, where a ^{14}C date of 7500 ± 90 cal. yr B.P. was obtained on shells (Figs. 3 and 6A; Table 1).

In general, the thicknesses of successions 1 and 2 are the same and thicker than that of succession 3. In addition, the grain size, thickness, and proportion of sand layers within each succession become progressively finer, thinner, and less abundant from succession 1 through succession 2 to succession 3, generating an overall upward-fining trend that is shown more conspicuously in the landward ZK02 core, but that is present also in core ZK01 (Fig. 3). Also, there is an increase in the abundance of some deeper-water foraminiferal fossils (e.g., *Nonionellina atlantica*, *Bolivina robust*, *Bulimina marginata*, and *Astrononion tasmanensis*) from succession 1 through succession 2 to succession 3 (Fig. 10).

In conclusion, the coarsening- and sandier-upward trend, and the stacking of depositional environments within each succession indicate a progradational nature, and the contacts between the successions abruptly place a deeper-water, more distal environment on top of a more proximal deposit. Thus, each succession represents a parasequence (cf. Catuneanu, 2006), which are separated by flooding surfaces marked by the abrupt changes in the depositional facies and

foraminiferal fossil content. Because each successive parasequence contains more distal and finer-grained deposits, the transgressive interval as a whole represents a retrogradationally stacked (i.e., back-stepping) parasequence set.

DISCUSSION

Tide-Dominated Deltaic Nature of the Studied Deposits

Because the same tidal sedimentary structures (e.g., double mud drapes, herringbone cross-stratification, etc.) and facies (e.g., tide-influenced fluvial channels, tidal channels, and tidal bars) can form in both tide-dominated deltas and estuaries (Dalrymple, 2010), interpretation of the larger depositional environment based only on these features is difficult or impossible. Instead, the spatial and temporal depositional trends related to variations in water depth, accommodation, relative intensity of physical processes, and suspended-sediment concentrations within the large-scale sedimentary system need to be assessed (Dalrymple et al., 1992, 2012;

Dalrymple and Choi, 2007; Legler et al., 2013), because tide-dominated estuaries and deltas are distinctive in terms of sediment-transport pathways and facies stacking patterns (Dalrymple, 2010; Dalrymple et al., 1992, 2012; Dalrymple and Choi, 2007; Chen et al., 2015).

With regard to the late Pleistocene to early Holocene transgressive deposits in the study area, the observations indicate that the sediments in the landward ZK02 core are sandier and of a more proximal character with regard to depositional environment than those of the equivalent unit in the seaward ZK01 core. For instance, succession 1 in the landward ZK02 core is characterized by the coarsest amalgamated fluvial-channel deposits (F1; Figs. 3 and 5A), whereas the contemporaneous unit in the seaward ZK01 core is dominated by finer-grained, heterolithic tidal-channel deposits (F3 and F4; Figs. 3 and 7). The tidal-channel-floor deposits (F3 and F4a) of succession 2 in the landward ZK02 core primarily consist of structureless or contorted silty sand and gravelly sand beds (Figs. 3 and 4D; 46.35–47.00 m depth in Fig. 6A), whereas the channel-bottom sediments of the correlative unit in seaward core ZK01 are dominated by sandy silt beds (Fig. 3). Similar, but less pronounced changes in sand grain size also occur in succession 3, with fine sand layers present in core ZK02 but absent in core ZK01. In all of the units, wave-influenced distal muddy deposits that contain wave-generated fluid-mud (DM) layers (F5a and F5b; Figs. 3 and 7) occur commonly in the seaward ZK01 core but are absent in the landward core (Fig. 3). Indeed, such a seaward-fining trend has been noted in the previous studies on the unit of interest (e.g., Hori et al., 2001a, 2002b; Li et al., 2000, 2002; Chen et al., 2003; Xu et al., 2016). This grain-size pattern is expected in deltaic systems because of the lack of accommodation landward of the shoreline and the export of river-supplied sediments to the mouth-bar area (cf. Dalrymple and Choi, 2007; Dalrymple, 2010; Fig. 9). By contrast, estuaries typically exhibit a coarse-fine-coarse grain-size distribution (Dalrymple et al., 1992, 2012), because they receive sediment from two sources: sediment supplied directly by the river, which becomes finer in a seaward direction, and coastal and seafloor sediments that are transported landward by flood-dominant tidal currents or waves, resulting in the existence of a bed-load convergence located in the meander-bend zone of tidal-fluvial channels in the inner part of tide-dominated estuaries (Dalrymple et al., 1992, 2012; Dalrymple and Choi, 2007). The sandy estuary-mouth deposits that would be expected if the system were an estuary are absent in the succession under study here.

Furthermore, the pervasive and diverse occurrences of tide- (OM2) and wave-generated (DM) fluid-mud layers, especially the DM layers that occur in the distal muddy deposits in the tide-dominated late Pleistocene to early Holocene paleo-Changjiang system, also suggest a deltaic nature, because their distribution has an intimate relationship with the location of the turbidity maximum zone (Jaeger and Nittrouer, 1995; Kuehl et al., 1996; Kineke et al., 1996; Dalrymple et al., 2003; Ichaso and Dalrymple, 2009; Mackay and Dalrymple, 2011; Wu et al., 2012). The turbidity maximum zone generally lies in the middle part of estuaries (namely, near the bed-load convergence), but it is located more distally in deltas, lying in the delta-plain and mouth-bar regions (Figs. 9A, 9D, and 9E; cf. figs. 9C and 11C *in* Dalrymple and Choi, 2007). As a result, the seaward part of estuaries is generally mud-free (Dalrymple et al., 1992, 2012; Chen et al., 2015), except in the cases where mud is supplied from a nearby large river, such as the modern Qiantang River estuary (Zhang et al., 2014), the Charente estuary (Chaumillon and Weber, 2006), and the Vilaine estuary (Tessier, 2012). Such an updrift source of mud does not exist for the paleo-Changjiang system. By comparison, the area seaward of the river mouth in deltas is characterized by muddy prodeltaic deposits that are supplied by the river itself (Fig. 9; Hori et al., 2002b; Dalrymple et al., 2003; Wang et al., 2005; Dalrymple and Choi, 2007; Bhattacharya, 2010). Thus, tidally generated fluid-mud (OM2) layers generally occur in the middle part of estuaries, if they are present at all, whereas such thick tidal mud layers are more abundant in deltas and occur in the tidal channels of delta-plain and delta-front areas (Figs. 9A, 9B, and 9C), as is the case in the paleo-Changjiang deposits. In addition, due to the irregular influence of storm waves in delta-front and prodelta areas (Figs. 9A, 9D, and 9E), resuspension of large amounts of preexisting mud leads to the formation of wave-generated fluid muds (DM layers; Figs. 9A, 9B, and 9C), as is the case in the offshore continental shelf of the Amazon River (cf. Jaeger and Nittrouer, 1995; Kuehl et al., 1996; Kineke et al., 1996), Eel River continental shelf (Hill et al., 2007), the modern Fly River delta (Dalrymple et al., 2003), and especially the modern Changjiang delta (Fig. 8; cf. Hori et al., 2002b; Wang et al., 2005).

The last and most important distinction between deltas and estuaries lies in the identification of the facies stacking pattern (Dalrymple and Choi, 2007; Bhattacharya, 2010; Feldman and Demko, 2015). The three coarsening- and sandier-upward parasequences (i.e., successions) that occur within the late Pleistocene to early Holocene paleo-Changjiang system indi-

cate a progradational nature, which is typical of deltaic systems. This is shown most obviously in succession 1 in core ZK01, which begins with distal muddy deposits, passes upward into tidal-bar deposits, and is truncated by tidal-channel deposits (Figs. 3 and 7), a succession that is common in the mouth-bar area of tide-dominated deltaic systems such as those in the Jurassic Tilje Formation, Norway (Ichaso and Dalrymple, 2014; Ichaso et al., 2016), and the modern Fly River (Dalrymple et al., 2003) and Changjiang deltas (Fig. 8; Hori et al., 2002b). Progradation in the form of seaward-dipping reflections is also evident in seismic sections imaging deposits that lie immediately below the present-day prodeltaic sediments. These progradational deposits have ^{14}C dates between ca. 12 cal. k.y. B.P. and 7.5 cal. k.y. B.P. (Unit II in Xu et al., 2016; see locations in Fig. 1) and hence correspond temporally to the three successions documented in our cores (Fig. 3). The seaward-dipping reflectors resemble the reflection characteristics of the modern Changjiang delta and downlap and/or onlap against older deposits, testifying to the deltaic origin for the paleo-Changjiang deposits (cf. Dalrymple et al., 1992, 2003; Feldman and Demko, 2015). The three obvious parasequences, which are separated by flooding surfaces and display an overall fining-upward trend (Fig. 3), indicate the long-term back-stepping nature of the study interval, which was punctuated by progradational episodes (cf. Dalrymple et al., 2012; Legler et al., 2013; Chen et al., 2015).

Based on this discussion, the late Pleistocene to early Holocene transgressive deposits in the Changjiang incised valley are interpreted to represent a back-stepping, tide-dominated deltaic system rather than an estuarine succession (Figs. 9 and 11). Thus, the tidal-channel deposits (e.g., F3 and F4) recognized above are distributary/terminal distributary channels, and the distal muddy deposits (F5a) are prodeltaic deposits.

Controls on the Evolution of the Paleo-Changjiang Delta

The sedimentary facies comprising the late Pleistocene to early Holocene transgressive deposits in the Changjiang incised-valley fill accumulated discontinuously rather than uniformly, especially during the existence of the paleo-Changjiang delta system, which is characterized by a combination of progradation (rapid sedimentation generating parasequences) and back-stepping marked by flooding surfaces (slowed or no sedimentation at the core site; Fig. 3). The fundamental factor determining the facies stacking pattern (regressive or transgressive) is the ratio between the rates of the

TABLE 3. DESCRIPTIONS AND INTERPRETATIONS OF THE FIVE ENVIRONMENTALY SIGNIFICANT FACIES IDENTIFIED IN THIS STUDY

Subfacies	Description	Sedimentary structures	BI and fossils	Interpretation
Facies 1 (F1): Coarser-grained structureless sand				
	3–13 m thick. Composed mainly of gravelly sand, sandy gravel, coarse or medium sand, without mud layers. Sands are the coarsest in the succession, dominated by coarse and medium sand, with lesser amounts of very coarse and fine sand, and minor granules. Gravels are angular to subangular and 2–50 mm in diameter. Sparse mud rip-up pebbles (~10%, diameters > core diameter), pieces of wood, and reddish-brown oxide stains are scattered throughout.	Erosionally based. Generally homogeneous, crude parallel lamination and cross-bedding present locally, probably because of coring disturbance. Consists of several fining-upward successions, each 0.5–3.0 m thick. Tidal structures are absent.	Bioturbation is not present (BI 0), and foraminiferal fossils are absent, except within the mud rip-up pebbles. Some intact gastropod fossils are scattered, including *Gyraulus* sp., *Tulotomoides* sp., and *Gyraulus cf. Planoconcavus* Gu and Wang, 1989.	The stacked nature of upward-fining successions with erosive bases, the presence of the coarsest grain sizes and freshwater gastropod fossils, and the absence of marine fossils and tide-influenced sedimentary structures indicate that F1 represents amalgamated fluvial-channel sediments deposited upstream of the tidal and salinity limits.
Facies 2 (F2): Alternation of coarser-grained structureless sand and heterolithic stratification				
	3–8 m thick. Characterized by the alternation of structureless sand beds (0.1–1.5 m thick; probably caused by coring disturbance) and heterolithic stratified intervals (0.3–1.0 m thick). The structureless sand beds consist mainly of silty sand and silty fine sand with minor gravel-bearing coarse sand (gravel comprising 5%–10% with clasts 2–5 mm in diameter), and mud rip-up pebbles. The heterolithic intervals show alternations of fine sand or sandy silt (2–20 mm thick; content 30%–70%) and OM1 layers (2–8 mm thick), locally with abundant terrestrial organic materials.	Erosionally based. Crude parallel lamination and unidirectional cross-bedding occur sporadically in the structureless sand beds. The double mud drapes, thick-thin alternations, and sandier-muddier intervals are present within the heterolithic intervals.	Bioturbation is absent (BI 0). Benthic foraminifera (BF) dominated by *Ammonia beccarii* vars. are encountered sporadically in the heterolithic stratification, but are absent in structureless sand beds. Some intact gastropod fossils dominated by *Tulotomoides* sp. present sporadically in structureless sand beds.	The structureless sands are interpreted to be accumulated in a fluvial-dominated channel, as indicated by the erosive-basal surface, the presence of coarser-grained sand and freshwater gastropod fossils, and the absence of tidal structures and marine fossils. The occurrence of double mud drapes, evidence of diurnal inequality (i.e., thick-thin alternations), and neap-spring rhythmic lamination (i.e., sandier-muddier intervals) within some of the heterolithic intervals indicate that tidal currents were present and were more intense than fluvial currents during the deposition of heterolithic deposits. The alternation of sand and heterolithic strata represents river-flood/interflood cycles. The scarcity of bioturbation, sporadic presence of foraminifera and freshwater gastropod fossils, thinness of mud layers, local enrichment of terrestrial organic material, and the alternation of periods of river and tidal dominance show that F2 represents the deposits of tidally influenced fluvial channels.
Facies 3 (F3): Finer-grained structureless sand and/or contorted deposits				
Facies 3a (F3a): Finer-grained structureless sand	Generally 0.5–1.0 m thick. The sand layers consist of well-sorted, fine and very fine sand (mean grain size of 3.32–4.30Φ), with lesser amounts of medium and coarse sand. Mud rip-up pebbles (diameters 0.5–4.0 cm; content 10%–30%) are common, especially above the erosive bases and showing an upward decrease in abundance and grain size.	Erosive contacts with the under- and overlying deposits. Generally structureless. Large-scale cross-beds occur sporadically in the lower part.	BI = 0. Benthic foraminifera (27–37 species per 50 g dry sample) are abundant, consisting principally of *Ammonia beccarii* vars., *Epistominella naraensis*, *Elphidium magellanicum*, *Cribrononion vitreum*, *Quinqueloculina* sp., and *Elphidium advenum*. Some abraded bivalves present.	The erosional basal contact, the presence of cross-bedding, the upward decrease in the abundance of mud rip-up pebbles, the meter-scale contorted bedding (F3b), and the ubiquitous presence of euryhaline and stenohaline benthic foraminifera similar to those in the (terminal) distributary channels of the modern Changjiang delta suggest that F3 represents tidal-channel-floor deposits.
Facies 3b (F3b): Contorted muddy or sandy deposits	Usually <1 m thick and comprising 0%–80% of sand layers. Characterized by contorted, interlaminated, or interbedded mud and sand and/or intermixed sand and mud deposits; unable to distinguish the original sedimentary layering and structures.	Erosive upper and lower contacts. Contorted bedding (i.e., slump deposits) in meter-scale are common.		

(continued)

generation of accommodation (*A*) and sediment supply (*S*; i.e., the *A/S* ratio; Hori et al., 2002a, 2002c; Catuneanu, 2006). Back-stepping parasequence sets like that documented here in the paleo-Changjiang deltaic succession can occur during transgression, as long as the *A/S* ratio is periodically less than 1 during a longer interval in which the ratio is close to but greater than 1. In this situation, the parasequences correspond to periods of slower relative sea-level rise or a higher sediment supply (local or more generally), whereas the bounding flooding surfaces form at times of more rapid relative sea-level rise or reduced sediment supply. In contrast, a classic estuarine valley-fill succession forms in transgressive settings when the *A/S* ratio is constantly larger than 1. The controls on the rates of sediment supply (*S*) and the generation of accommodation (*A*) can be either externally imposed (i.e., allogenic; relative sea-level change in response to eustatic sea-level

TABLE 3. DESCRIPTIONS AND INTERPRETATIONS OF THE FIVE ENVIRONMENTALY SIGNIFICANT FACIES IDENTIFIED IN THIS STUDY (*continued*)

Subfacies	Description	Sedimentary structures	BI and fossils	Interpretation
Facies 4 (F4): Bedded/laminated heterolithic stratification				
Facies 4a (F4a): Fining- and thinning-upward heterolithic stratification	Generally <1 m thick. Characterized by the alternation of sand or sandy silt and OM2 layers, commonly displaying a thinning-upward trend for both the sand and mud layers, especially for the mud layers, and fining-upward trend for sand layers, generating an overall sandier-upward succession. Sand, which constitutes <50% of F4a, ranges from coarse sand to silt, sporadically with granules, and generally occurs as thick laminae (usually <1 cm thick), but could locally be present as thick beds with thicknesses reaching up to 15 cm.	Erosively based. Small load structures are present at the base of many sand layers. Asymmetric ripples are pervasive at the top of sand layers; symmetrical ripples are less abundant.	Scarce bioturbation is commonly present at the top of OM2 layers with a BI of 0–1. Foraminiferal fossils abundant and are mainly composed of benthic foraminifera (28–42 species per 50 g dry sample), dominated by *Ammonia beccarii* vars., *Elphidium magellanicum*, *Epistominella naraensis*, *Cribrononion vitreum*, *Elphidium nakanokawaense*, *Florilus decorus*, *Protelphidium tuberculatum*, and *Elphidium advenum*.	The presence of an erosional base and OM2 fluid-mud layers in association with coarse-grained sand, and coexistence of euryhaline and stenohaline benthic foraminifera similar to those in the (terminal) distributary channels of the modern Changjiang delta indicate that F4a represents tidal-channel-floor deposits formed beneath the TMZ. The upward thinning of OM2 and upward-sandier nature of F4a reflect an upward decrease of SSCs within the channel, whereas the upward thinning and fining of sand layers indicate the progressive decrease of current speed upward within the channel.
Facies 4b (F4b): Coarsening- and thickening-upward heterolithic deposits	Usually <1 m thick. Consisting of a coarsening- and sandier-upward succession, from the thinly to thickly laminated sandy silt and OM1 (locally OM2) layers in the lower part, through silty fine sand in the middle, to structureless medium and fine sand on the top.	Erosively based. Sand-mud couplets occur in the lower part. Herringbone cross-stratification is present within the middle part.	Bioturbation is scarce with a BI of 0–1. Foraminiferal content not known.	The presence of sand-mud couplets (i.e., tidal rhythmites), herringbone cross-stratification, and a coarsening- or sandier-upward succession indicate that F4b may represent the bottomset or toeset portion of compound dunes in a channel-axis location, based on the muddy nature of the deposits and the presence of fluid-mud (OM2) layers.
Facies 5 (F5): Alternation of laminated heterolithic stratification and DM layers				
Facies 5a (F5a)	The laminated heterolithic stratification consists of alternation of sand or silt layers (1–35 mm thick, 30%–80% by volume) and OM1 or OM2 layers (3–30 mm thick), especially the OM1 variety, locally showing quasiregular muddier-sandier intervals. DM layers are 5–30 cm thick and comprise >70% by volume in F5a.	Wavy, lenticular, and flaser bedding are common in the laminated heterolithic stratification. Current-ripple cross-lamination is pervasive in sand layers. DM layers are generally homogeneous, sporadically with faint horizontal layering and obvious breaks.	Bioturbation is generally present on the top of DM layers with a BI of 0–1 in F5a and F5b, but is slightly more abundant in F5c with a BI of 1–3. Foraminifera fossils dominated by BF are also abundant in F5 (13–44 species per 50 g dry sample), and are characterized by *Ammonia beccarii* vars., *Epistominella naraensis*, *Florilus decorus*, *Elphidium magellanicum*, *Quinqueloculina* sp., *Cribrononion vitreum*, *Nonionellina atlantica*, and *Nonionella jacksonensis*. In general, the average proportion for *Ammonia beccarii* vars. decreases from 31% in F5b and F5c to 23% for F5a, and the content of deep-water species (such as *Epistominella naraensis*, *Quinqueloculina* sp., *Nonionellina atlantica*, and *Nonionella jacksonensis* (water depth >30 m) has an inverse tendency.	Based on the differences in mud-layer type, F5 reflects the alternation between times of tide domination (laminated heterolithics containing OM1 and OM2 layers) and wave domination (DM layers; storm deposits). The quasiregular muddier-sandier laminated intervals indicate neap-spring cycles. In addition, because wave energy decreases landward due to friction, and mud resuspended by waves tends to flow downslope, F5a can be interpreted as prodeltaic sediments formed in the mouth of the system where wave action was episodically intense, yet tidal currents dominated sedimentation most of the time, and F5b and 5c represent tidal-bar deposits located at intermediate elevations adjacent to the tidal channels where it was not as favorable for the accumulation of abundant fluid-mud deposits. F5b, with its greater abundance of DM layers, is interpreted to have formed more seaward and/or deeper than F5c. The relatively higher content of deep-water foraminiferal fossils in F5a and F5b also strengthens this interpretation.
Facies 5b (F5b)	Similar to F5a, but the content of DM layers in F5b is 30%–50%.			
Facies 5c (F5c)	Similar to F5a and F5b, but the content of DM layers in F5c is <30%.			

Note: BI—bioturbation index; SSCs—suspended-sediment concentrations; TMZ—turbidity maximum zone; OM1—organized-mud type 1; OM2—organized-mud type 2; DM—disorganized mud. See more details about the mud-layer types in Table 2.

rise and tectonic subsidence, and climatically driven changes in sediment supply), or of local origin (i.e., autogenic; delta-lobe switching and compaction-driven subsidence). Whereas the allogenic causes are likely to have a regional impact on sedimentation, delta-lobe switching as a result of avulsions (cf. Slingerland and Smith, 2004) will have a more localized influence on the *A/S* ratio by changing the location of sediment input, leading to lobe progradation at a site when the river mouth is nearby and transgressive ravinement during periods of abandonment. Such alternations of progradation and transgression in response to avulsions have been widely documented in modern

deltas, such as the river-dominated Mississippi River delta (Fisk and McFarlan, 1955; Blum and Roberts, 2012) and the Yellow River delta (Qian, 1990; Liu et al., 2010), as well as the tide-dominated Ganges-Brahmaputra River delta (Goodbred and Kuehl, 2000a), Fly River delta (Dalrymple et al., 2003), Mahakam Delta (Gastaldo et al., 1995), and the Eocene Lower Dir Abu Lifa member, Western Desert, Egypt (Legler et al., 2013). Separating the effects of allogenic and autogenic controls on the stratigraphy is difficult in the present case because of the relatively small number of cores available in this study. Nevertheless, some preliminary interpretations are possible.

In the unit of interest, most amalgamated fluvial-channel deposits (F1) are thought to have been deposited by aggradation during the initial stage of the transgression, after the LGM and before 13,500 ± 180 cal. k.y. B.P. (cf. Li et al., 2000, 2002, 2006; Table 1; Figs. 3 and 11), which may be related to the lower rate of the relative sea-level rise during the 18.5–15.4 cal. k.y. B.P. period (SRP I, ~5 mm/yr; Fig. 11) caused by the Older Dryas cooling event (Koutavas et al., 2002; Li et al., 2014). The transgressive surface (TS) located within F1 may have resulted from the abrupt sea-level rise during RRP I (19.0–18.5 cal. k.y. B.P.; ~20 mm/yr; Fig. 11) ascribed to the rapid melt of ice cap (Li et al., 2014).

Figure 8. Photographs from core ZK02 showing the prodelta to delta-front deposits of the modern Changjiang delta (depth in m). The prodelta deposits (F5a; 27.00–29.00 m depth) are mainly composed of disorganized mud (DM) layers, which are separated by subtle breaks. Sand is scarce. Bioturbation (B) is generally absent, but locally can be abundant (e.g., at 27.40–27.65 m depth). This facies can be compared with F5a of the paleo-Changjiang delta (see 66.82–68.00 m depth in Fig. 7). The delta-front deposits are characterized by heterolithic tidal-bar deposits (F5b), punctuated by tidal-channel-floor deposits (F3a and F4a) that resemble those of the paleo-Changjiang delta (see 60.00–67.00 m depth in Fig. 7). The tidal-bar deposits (F5b; 24.42–25.00 m and 26.00–26.74 m depth) are mainly composed of the alternation of tidal rhythmites and DM mud layers. The tidal-channel-floor deposits occur as structureless sand with broken shells and mud rip-up pebbles (MRP; F3a; 24.00–24.42 m and 26.74–27.00 m depth), or thin-bedded heterolithic stratification (F4a; 25.00–26.00 m depth) composed mainly of organized mud (OM2) layers, with a few DM layers indicating episodic wave influence.
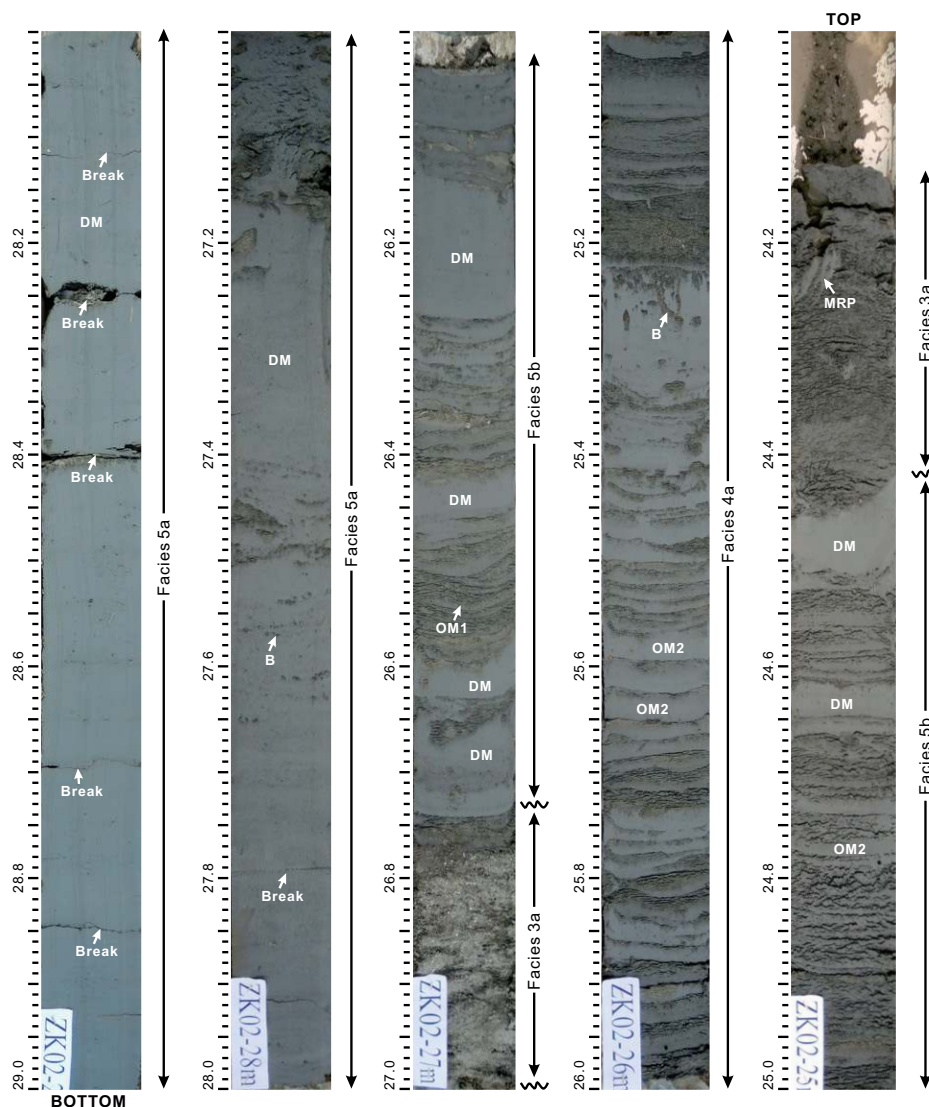
Figure 9 (*on following page*). (A) Schematic of the environmental distribution within the late Pleistocene to early Holocene paleo-Changjiang delta in plan view, showing the positions of the constituent geomorphological elements. Note that the subaqueous tidal bars are the seaward extension of the subaerial tidal bars and islands. BLC—bed-load convergence. (B) Longitudinal distribution of the relative abundance of sand and mud, of the sand grain size (indicated schematically by the size of particles), and of the mud-layer types (OM1, OM2—organized mud layers types 1 and 2; DM—disorganized mud layers). (C) Longitudinal change in the nature of the sedimentary successions at different morphologic positions in response to the variation in the physical processes and suspended-sediment concentrations. Numerical labels for vertical columns correspond to numbers in A and D. Columns ① and ② represent successions mainly composed of amalgamated fluvial-channel deposits (F1), indicating the dominance of fluvial currents. Succession ③ contains F2 (tide-influenced fluvial channel), which is characterized by the alternation of structureless sand (river-flood deposits) and laminated (tidal) heterolithics (interflood deposition). Columns ④ to ⑥ consist primarily of distributary-channel-floor (F3 and F4a) and adjacent tidal-bar (F5b and F5c) deposits, with tidal currents as the major physical process, sporadically influenced by storms. Column ⑦ represents the typical succession in the delta-front area, which is characterized by muddy tidal-bar deposits (F5b) punctuated by terminal-distributary-channel-floor deposits (F3 and F4), with abundant disorganized mud (DM) layers, indicating the significant influence of storms. Succession ⑧ consists of prodeltaic muddy deposits (F5a), which are predominantly composed of DM layers. (D) Simplified schematic representation of the change in the nature of current patterns over a tidal period in the fluvial-marine transition zone. F—landward-directed flood currents or wave action; E—seaward-directed (river and/or ebb) currents. (E) Longitudinal distribution of energy types and suspended-sediment concentrations (SSCs) through the fluvial-to-marine transition. Parts A, B, D, and E are modified after Dalrymple and Choi (2007).

Figure 9.
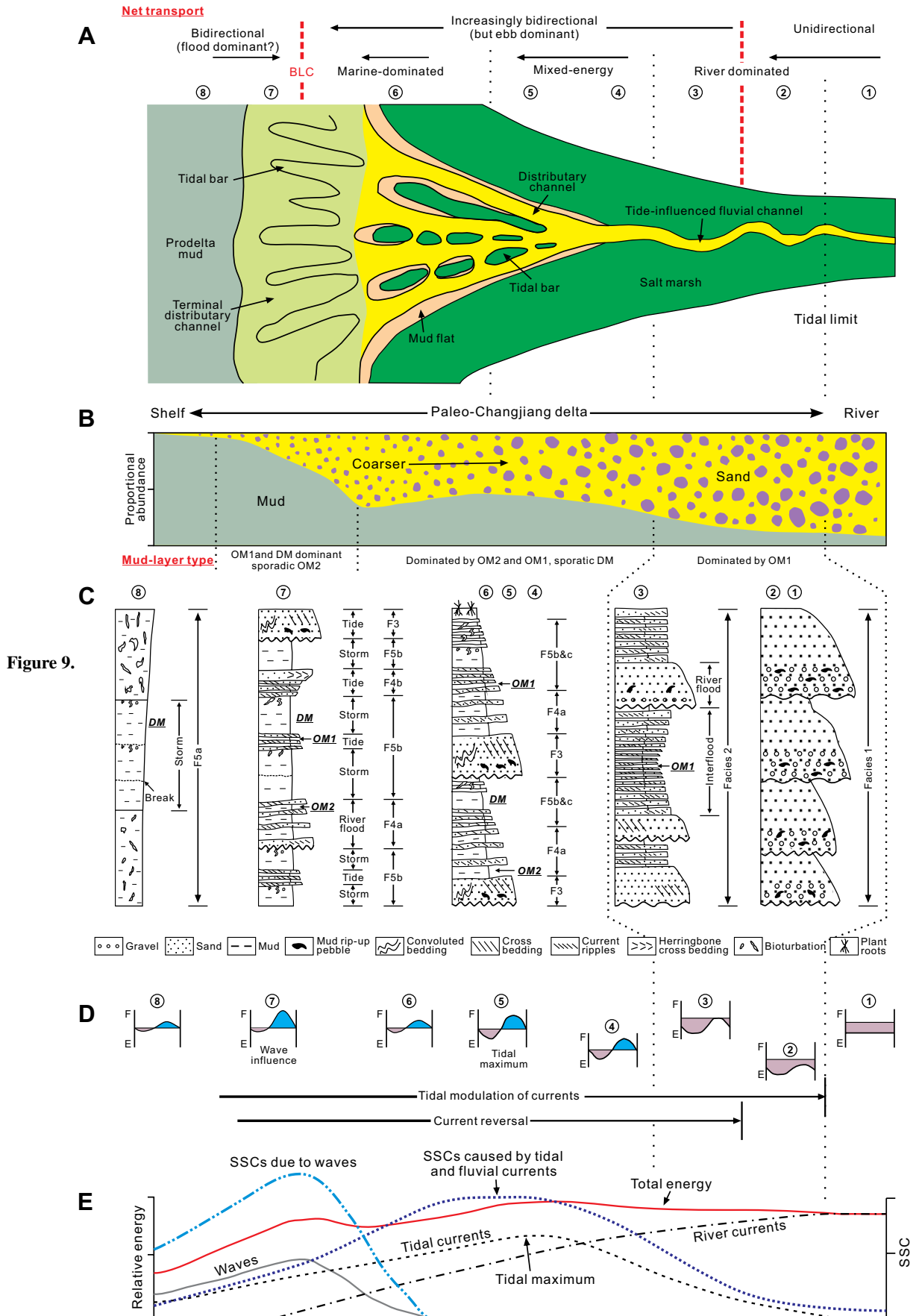
As for the overlying unit of tidal fluvial-channel deposits (F2), it was formed before 13 cal. k.y. B.P., and it is bounded by two flooding surfaces (FS1 and FS2; Figs. 3 and 11; Table 1) that were likely generated in response to the second rapid rise of relative sea level during the 15.4–13.0 cal. k.y. B.P. period (RRP II, ~15 mm/yr; Fig. 11) that was caused by meltwater pulse 1a and the Bølling-Allerød (BA) and Termination-1a warming events (Deschamps et al., 2012; Li et al., 2014). The first one (FS1), which was generated in the initial part of this period, is a relatively small back-step with F2 overlying F1, but the second one (FS2), which formed during the final part of this period, is a much bigger translation causing prodeltaic deposits (F5a) to rest on F2 in core ZK01. Such back-stepping has also been reported in previous publications, based on rapid facies changes in cores from both the East China Sea continental shelf and areas landward of our cores, and it is also recorded by truncated reflections seen in seismic profiles obtained from the modern subaqueous deltaic area (cf. Tang, 1996; Hori et al., 2002b; Xu et al., 2016).

The coarsening- and sandier-upward succession 1 accumulated after the formation of FS2 and before ca. 11 cal. k.y. B.P. (Figs. 3 and 11; Table 1; cf. Hori et al., 2001a). It is likely that allogenic factors contributed to the progradation of succession 1, specifically, some combination of the relatively slower rate of relative sea-level rise (6 mm/yr associated with SRP II, 13.0–11.0 cal. k.y. B.P.), which may have been caused by the Younger Dryas cooling event (Fairbanks, 1989; Koutavas et al., 2002; Liu et al., 2010; Li et al., 2014; Xu et al., 2016), and an increased riverine sediment supply ascribed to the significantly enhanced Asian summer monsoon during the early Holocene throughout the tropics and subtropics (Goodbred and Kuehl, 2000b; Chen et al., 2005), which resulted in increased precipitation during the flood season over the Tibetan Plateau region around 12.0 ka (Winkler and Wang, 1993). However, the relative importance of these two allogenic factors in the generation of succession 1 is unclear. Succession 1 is terminated by a third small-scale flooding surface (FS3), which can also be recognized in the more proximal HQ98 and JS98 cores (cf. Hori et al., 2002b, 2002c) and in the seaward ZK9 core (Wang et al., 2010). This flooding surface may correlate to the abrupt sea-level rise with a rate of more than 28–45 mm/yr shortly after 11.0 cal. k.y. B.P. (RRP III; Fig. 11) due to meltwater pulse 1b, associated with the Termination-1b warming event (Fairbanks, 1989; Rühlemann et al., 1999; Hori et al., 2002b).
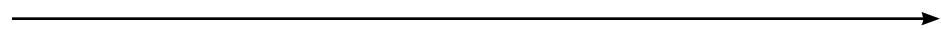
Succession 2 rests on FS3 and appears to have formed during the period of 11–9 cal. k.y. B.P. (Figs. 3 and 11; Table 1). There was no significant reduction in the rate of sea-level rise during this period (RRP III, 11.0–9.3 cal. k.y. B.P.; Fig. 11; Li et al., 2014). However, a humid, wet, and warm climatic interval occurred and peaked ca. 11.4–9.0 cal. k.y. B.P., in association with a rapid rise in temperature on the Tibetan Plateau (Chen et al., 2005; Yi et al., 2006; Wang et al., 2010; and references therein), which may have led to the progradation of succession 2 by causing an increase in the rate of sediment supply that overwhelmed the rapid rise of sea level. Succession 2 is bounded at its top by FS4, which is probably a product of the fourth large-scale sea-level jump (RRP IV; 9.0–8.0 cal. k.y. B.P.; ~30 mm/yr) due to the final collapse of the Laurentide ice sheet and the catastrophic draining of glacial lakes Agassiz and Ojibway (Tjallingii et al., 2014, and references therein). The effects of this rapid rise have been reported in many places, including the Changjiang, Red, and Kiso River incised valleys, the Yellow and Bohai Sea, the Rhine-Meuse and Mississippi deltas, New Zealand, and the central Great Barrier Reef among others (Hori and Saito, 2007; Hijma and Cohen, 2010; Wang et al., 2012a; Tjallingii et al., 2014, and references therein), and it may be the major reason that the depocenter of the paleo-Changjiang delta moved rapidly landward such that prodelta to delta-front deposits at the base of succession 3 rest on the delta-plain deposits at the top of succession 2 (Figs. 3 and 11).

Subsequently, succession 3 accumulated during ca. 9.0–7.5 cal. k.y. B.P. (RRP IV; Figs. 3 and 11; Table 1). A small-scale decrease in the rate of sea-level rise, which may have been related to the 8.2 ka cooling event (Fig. 11; Hijma and Cohen, 2010; Li et al., 2014) ,presumably facilitated the progradation of succession 3, but there were also climatic fluctuations that might have contributed to more rapid sedimentation, although the details of the climatic changes during this period are uncertain, with different workers proposing different climatic scenarios (cf. Chen et al., 2005; Tao et al., 2006; Yi et al., 2006; Wang et al., 2010, and references therein).

Compared to succession 1, the links between the progradational events that generated successions 2 and 3 and allogenic causes are much less obvious because the rate of relative sea-level rise was generally high during the formation of successions 2 and 3 without pronounced fluctuations (Fig. 11), and the climate-driven impact on variations in the rate of sediment supply is ambiguous. Consequently, an autogenic origin (i.e., avulsion) may have been responsible for the generation of these two successions, the existence of which can be indirectly implied by the alternation between high (10–50 m/k.y.) and low (< 3 m/k.y.) sedimentation rates documented by Feng et al. (2016) and Xu et al. (2016). In fact, large-scale river avulsion has been documented in the Changjiang system during the Quaternary (Fig. 12; Chen and Stanley, 1995; Schneiderman et al., 2003; Wellner and Bartek, 2003; Wang et al., 2012b). It has been proposed that the Changjiang flowed across the northern part of the northern flank of the modern delta, adjacent to Yancheng and Dongtai (Figs. 1 and 12), and discharged sediment to the southern Yellow Sea during much of Quaternary time (Chen and Stanley, 1995; Schneiderman et al., 2003; Wellner and Bartek, 2003), resulting in the presence of a large, former deltaic system in the northern part of the northern flank and its submarine extension (cf. Zhu et al., 1984). Since the early Pleistocene, the Changjiang has shifted southward; the main distributary channels were located around the apex of the Jianggang radial tidal sand ridge field during the late Pleistocene (Fig. 12), the presence of which exerted a significant role in the formation of the radial tidal sand ridges after the delta was abandoned (Wang et al., 2012b). The main channel of the Changjiang then switched to its modern, southerly course in the late Holocene (Fig. 12; Chen and Stanley, 1995; Schneiderman et al., 2003). Additionally, evidence of smaller-scale avulsions and channel abandonment is also provided by the presence of six delta lobes that form the en echelon succession of river-mouth bars along the northern margin of the modern channel, which has shifted and prograded southeastward progressively since 8.0 cal. k.y. B.P., with channel and mouth-bar abandonment occurring at intervals of ~1000–2500 yr (Fig. 12; cf. Liu et al., 1992; Hori et al., 2001b; Li et al., 2000, 2002; Feng et al., 2016). The most recent avulsion was the abandonment of the North Branch of the modern Changjiang delta (Xu et al., 2016), in a process similar to the abandonment of the Far Northern Entrance of the modern Fly River

Figure 10. Down-core variations of foraminiferal species abundance in the ZK02 core. PF—planktonic foraminifera; BF—benthic foraminifera; *n*—number; FS—flooding surface; S1, S2, and S3—successions 1, 2, and 3, respectively. Black arrows show a decreasing-upward trend for the benthic and planktonic foraminifera abundance, and the content of benthic foraminifera species and specific foraminiferal fossils. See more details about the vertical log on the left and facies on the right in Figure 3A.
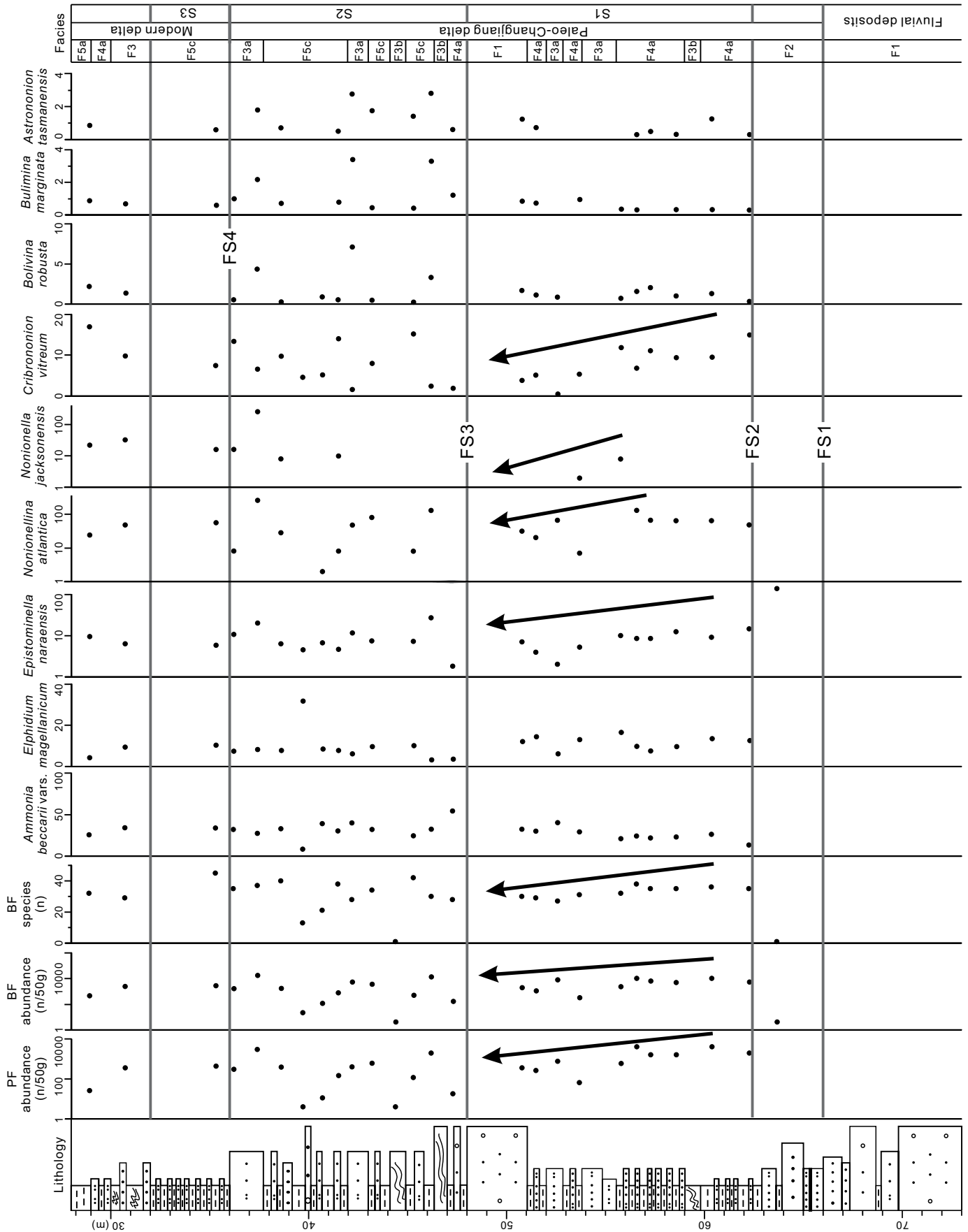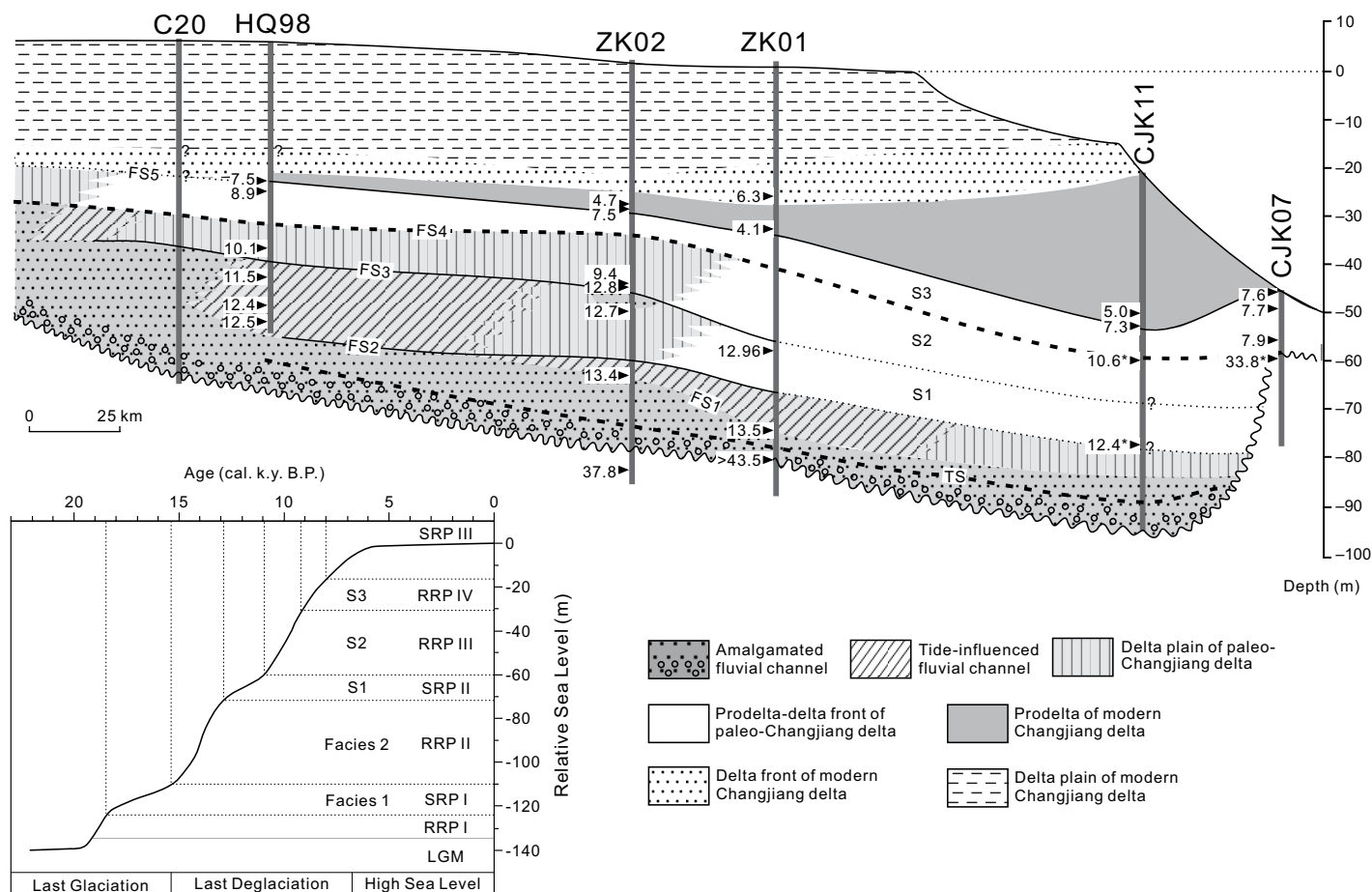
Figure 10.

Figure 11. Schematic dip-oriented cross section showing the interpreted stratigraphic organization of the paleo-Changjiang delta. FS—flooding surface; S—succession; LGM—Last Glacial Maximum; SRP—slow sea-level rise phase; RRP—rapid sea-level rise phase. Inset shows the relative sea-level curve for the postglacial period (modified from Li et al., 2014). Data from the C20, HQ98, and CJK11 and CJK07 cores were obtained and modified from Li et al. (2002), Hori et al. (2001a, 2002b), and Xu et al. (2016), respectively. All recalculated ^{14}C and optically stimulated luminescence (OSL; marked by *; Xu et al., 2016) ages are reported in (cal.) k.y. B.P. (see more details in Table 1). See core locations in Figure 1. TS—transgressive surface.

delta (cf. Dalrymple et al., 2003). Areas where the subdelta lobes form are characterized by a high sedimentation rate, whereas areas away from the river mouth, and especially in updrift locations (i.e., to the north), have a much lower sedimentation rate. For instance, the high sedimentation rates recorded in the upper ~20 m in cores HQ98, JS98, and CM97 correlate with the formation of the corresponding river-mouth bar (cf. table 3 *in* Feng et al., 2016). Similarly, the sedimentation rate was up to ~20 mm/yr in core CJK11 during 5.0–3.0 cal. k.y. B.P., when the adjacent mouth bar formed, whereas the other cores shown in Figure 1 in the subaqueous delta area had sedimentation rates that were less than ~3 mm/yr at the same time (cf. Xu et al., 2016). Also, the southward avulsion of the river mouth from Hongqiao to Huangqiao caused significant recent erosion in the northern part of the modern Changjiang delta (Fig. 12; Liu et al., 1992;

Wang et al., 2005), as shown by the absence of sediments deposited since ca. 7.5 cal. k.y. B.P. in core CJK07 and since ca. 6.5 cal. k.y. B.P. in core CJK08 (Fig. 11; see more details in figs. 7 and 9 *in* Xu et al., 2016). Therefore, if successions 2 and 3 were formed by river avulsions, then the formation of FS3 and FS4 may have resulted from transgressive erosion caused by some combination of abandonment of delta lobes and the rapid relative sea-level rise during this period.

As for the position of the maximum flooding surface, there are two possibilities. The maximum flooding surface has traditionally been placed on the top of succession 3, which is marked by an abrupt facies change, with prodeltaic mud of the modern Changjiang delta resting on the delta-front and prodeltaic deposits of the paleo-Changjiang delta, with an age of 7.5–8.0 cal. k.y. B.P. (cf. Hori et al., 2002a; Li

et al., 2002; Song et al., 2013; Li et al., 2014; Xu et al., 2016). The another option is the flooding surface at the top of succession 2 (FS4), which was created in response to the final period of rapid sea-level rise ca. 9.0–8.0 cal. k.y. B.P. In this paper, it seems more suitable to position the maximum flooding surface on the top of succession 2, since the turn-around from net transgression to sustained regression appears to occur at this point in the stratigraphic correlation shown in Figure 11, with delta-front and prodeltaic deposits extending farther landward than core C20 directly above FS4. Theoretically, the switch from transgression to regression happens earlier in situations where the sediment supply is larger, for a given rate of sea-level rise (cf. Catuneanu, 2006), as is the case with the Changjiang, which is one of largest rivers in the world. Indeed, the rate of relative sea-level rise was slowing by the time of formation of the FS4 (Fig. 11; Li et al.,
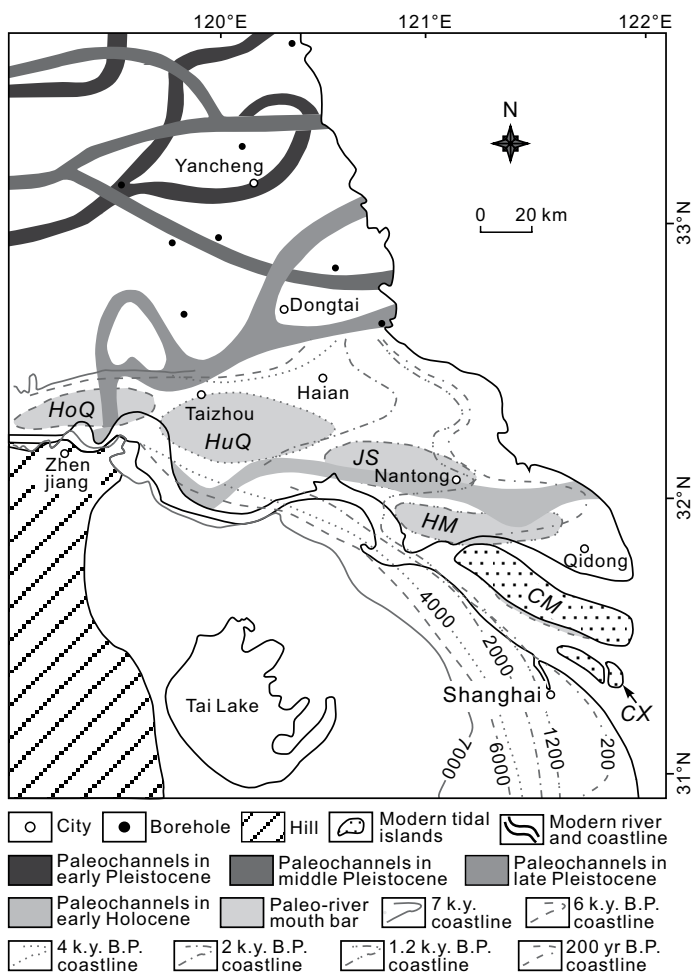
Figure 12. Map showing the distribution of Changjiang paleochannels from the early Pleistocene to the present. Also depicted is the reconstructed evolution of Holocene coastlines and river-mouth sand bars of the modern Changjiang delta during the past 7000 yr. Data were compiled and modified after Chen and Stanley (1995) and Hori et al. (2001b). HoQ—Hongqiao river-mouth sand bar; HuQ—Huangqiao river-mouth sand bar; JS—Jinsha river-mouth sand bar; HM—Haimen river-mouth sand bar; CM—Chongming river-mouth sand bar; CX—Chongxing river-mouth sand bar. See Figure 1 for the distribution of the main delta and the southern and northern flanks of the modern Changjiang delta.

Nevertheless, it is of note that the Changjiang has been capable of constructing a delta at its mouth since at least 13.0 cal. k.y. B.P.; during the initial period (prior to ca. 9.0 cal. k.y. B.P.), these deltas back-stepped, but continual progradation has occurred since ca. 9.0 cal. k.y. B.P. This new interpretation of the history of the Changjiang delta is obviously different from the commonly accepted view that the onset of delta formation in different parts of the world began ca. 8.5–6.5 k.y. B.P. (Stanley and Warne, 1994), and also from previous interpretations of the Changjiang that suggested that the maximum flooding surface formed at ca. 7.5–8.0 cal. k.y. B.P. However, large rivers with a high sediment load can easily create deltas within an overall transgressive setting, as is seen, for example, in the Ganges-Brahmaputra (Goodbred and Kuehl, 2000a) and Mississippi River deltas (Fisk and McFarlan, 1955). In the first case, an ~50-m-thick aggradational succession of lower delta-plain mud accumulated in the Bengal Basin due to the high rate of sediment input during the 11.0–7.0 k.y. B.P. period (2.5×10^9 t/yr, i.e., double the modern rate; Goodbred and Kuehl, 2000b), indicating relative shoreline stability during the initial formation of the Ganges-Brahmaputra River delta, despite the rapid sea-level rise of ~30–35 m at a mean rate of >10 mm/yr (Goodbred and Kuehl, 2000a). In the Mississippi River delta, the transgressive systems tract comprises three back-stepping shelf-phase delta lobes formed during the 9.0–3.5 k.y. B.P. period (Penland et al., 1988; Boyd et al., 1989).

Apparently, it is the immense sediment discharge of these large rivers that determines the early onset of delta formation. The main difference among the three major deltas is the relationship between the rates of relative sea-level rise and sediment supply. For the Ganges-Brahmaputra River delta, the sediment supply could keep pace with rapid accommodation production during the early Holocene transgression due to the stronger-than-present southwest monsoon and intense precipitation. However, for the Changjiang and Mississippi River deltas, the sediment supply was insufficient to balance the accommodation creation, and the deltas transgressed in a stepwise fashion in response to the fluctuating rates of relative sea-level rise, sediment supply, and avulsions. Consequently, considerable attention must be paid during the interpretation of ancient deposits because deltas do not form only during times of stable or falling relative sea level; they can also occur during times of rapidly rising sea level if the rate of sediment input exceeds the rate of creation of accommodation. Thus, not all transgressive successions need to have accumulated in an estuary (sensu Dalrymple et al., 1992).

2014), conditions that are conducive to the early onset of progradation of the modern delta. More work is needed to determine the age of the maximum flooding surface more exactly.

In summary, it is difficult to confirm with certainty the cause for the formation of the successions and the associated flooding surfaces within the transgressive succession, but the depositional conditions were clearly not steady, providing many possible causes for the existence of the parasequences and the stepped transgression. Although there is circumstantial evidence that some of the stratigraphic packages correlate temporally with changes in the rate of sea-level rise and climatically induced changes in sediment supply, and hence could be of allogenic origin, we are not able to exclude the possibility that some of the units owe their origin to avulsions. In addition, allogenic factors appear to have exerted their greatest control on the stratigraphic packaging when sea level was rising rapidly (i.e., during the early postglacial period), whereas during times of slower sea-level rise or sea-level stillstand, autogenic factors may have been relatively more important. More detailed work on climate, sea-level change, sedimentation rate, and river avulsions is needed to resolve the uncertainty.

Implication for Biogenic Gas Reservoir Performance

Common reservoirs within tide-dominated deltas include distributary channel fills, mouth bars, sandy delta fronts, and elongate tidal bars associated with the delta front (Dalrymple et al., 2003; Ichaso and Dalrymple, 2014; Feldman and Demko, 2015, and references therein). For the study interval, because of the high mud content, the key reservoir components are the purely fluvial channel deposits (F1), because of their relatively great thickness (3–13 m) and the absence of mud baffles or barriers. The more proximal variants of tide-influenced fluvial-channel sediments (F2) have moderate reservoir properties; the parts of this facies that were deposited during river floods (generally 0.1–1.5 m thick) are devoid of mud layers and could host hydrocarbons; however, they are interbedded with interflood deposits (~0.3–1.0 m thick) that are heterolithic with a mud content of 30%–70%. The proportion of muddy interbeds increases in a seaward direction. Most of channel-floor deposits (F3b and F4) in (terminal) distributary channels are heterolithic and characterized by abundant OM1 mud drapes or OM2 fluid-mud beds (usually 50%–70% by volume), or contorted bedding, resulting in poor reservoir characteristics. Only rarely is there a sandy channel-floor component in the delta-plain or mouth-bar areas (F3a; Fig. 6A) because of the abundance of fluid-mud deposits in this area. The heterolithic deposits of the tidal bars and prodelta (F5) have poor reservoir potential, because of the abundance (usually >50% by volume) and likely lateral continuity of mud layers. Shallow biogenic gas shows and permeability tests also confirm these assessments, with the channel sands of F1 and F2 being the main gas reservoirs and channel-floor sand (F3a) representing the secondary reservoir facies (Lin et al., 2015). The horizontal permeability of the sand deposits from F1 and F2 varies from 548.25 mD to 798.87 mD, and from 263.40 mD to 4039.75 mD, respectively, whereas the sand deposits from F3a have a range of 99.87–170.37 mD, with the low-permeability values probably due to the high abundance of mud rip-up pebbles (Lin et al., 2015; see 64–65 m depth in Fig. 7).

CONCLUSIONS

The late Pleistocene to early Holocene transgressive deposits in the postglacial Changjiang incised-valley fill are heterolithic and characterized by a diverse suite of mud-layer types comprising two varieties: organized (i.e., they show evidence of tidal rhythmicity; OM1 and OM2) and disorganized (i.e., randomly distributed; DM) mud layers. Mud layers of the former type were deposited during tidal slack-water periods when suspended sediment settled, whereas the latter type was generated by the deposition of storm-resuspended mud, and these are irregularly interspersed within intervals of tide-generated deposits. The OM2 and DM layers are interpreted as fluid-mud deposits on the basis of their thickness (>1 cm) and homogeneous nature. Their spatial and stratigraphic distribution in the study interval provides important information about the suspended-sediment concentrations and relative physical processes, which in turn constrains the environmental interpretation of these deposits (cf. Ichaso and Dalrymple, 2009; Mackay and Dalrymple, 2011; Dalrymple et al., 2003, 2015; van den Berg et al., 2007; Chen et al., 2015).

These mud-layer types, combined with the abundance and nature of the associated sand deposits, allow the definition of five genetically related environments: amalgamated fluvial channel (F1) characterized by coarse-grained structureless sand that lacks mud layers; tide-influenced fluvial channel (F2) distinguished by the alternation of homogeneous sand beds deposited during river floods and tidally laminated heterolithic deposits that accumulated during interflood periods; tidal-channel-floor deposits (F3 and F4) characterized by fine-grained structureless sand, and contorted or bedded/laminated heterolithic stratification with abundant OM2 layers; and tidal-bar and distal mud deposits formed at the mouth of a tide-dominated system (F5) typified by the alternation of wave-generated DM layers and tide-dominated heterolithic deposits with mud layers in which the OM1 variety dominates. Vertically, these sedimentary facies occur as three retrogressively stacked successions (each one 4–14 m thick) that, accompanied by the underlying F1 and F2, comprise an overall fining- and muddier-upward succession, indicating that the transgression occurred by episodic back-stepping in response to variations in the *A/S* ratio, which was apparently controlled mainly by externally imposed factors (i.e., variations in the rate of relative sea-level rise or climate-driven changes in the rate of sediment supply), although local, autogenic variations in the sedimentation rate (namely avulsions) may have been the cause for some of the stratigraphic packaging, especially those that formed as the rate of relative sea-level rise slowed. Each succession displays a coarsening-upward trend that reflects its progradational nature, which is also indicated by the seaward-dipping clinoforms that have been imaged seismically for the correlative interval located beneath the modern subaqueous delta. Longi-

tudinally, these facies present an overall fining-seaward trend, from the coarse sand or gravel of F1, to medium or fine sand in F2, to fine or very fine sand and silt in F3, F4, F5b, and F5c, and finally to mud-dominated distal deposits (F5a). The mud-layer types also display an obvious longitudinal trend, with OM1 layers present throughout the entire system, OM2 layers occurring widely in the tidal channels, and DM layers occurring only in F5, which formed in the exposed mouth of the system. All of these characteristics indicate that the investigated deposits formed in a deltaic environment (cf. Dalrymple et al., 2003, 2015; van den Berg et al., 2007; Ichaso and Dalrymple, 2009, 2014; Mackay and Dalrymple, 2011; Chen et al., 2015). Thus, at least the uppermost part of the late Pleistocene to early Holocene transgressive deposits in the study area (i.e., the heterolithic tidal deposits) represent a back-stepping, tide-dominated delta rather than an estuary, as previously thought. In this new interpretation, the tidal-channel-floor deposits (F3 and F4) are distributary/terminal distributary channels, and the distal muddy deposits (F5a) are prodeltaic deposits.

This study is consistent with sequence-stratigraphic principles, which indicate that the onset of deltaic sedimentation will occur earlier when the rate of sea-level rise is faster, in situations where the rate of sediment input is higher. We propose on the basis of the stacking pattern of the successions that the maximum flooding surface might have formed as early as ca. 9.0 cal. k.y. B.P., instead of at the commonly believed date of 7.5–8.0 cal. k.y. B.P. This study provides new insights into the nature of tide-dominated deltaic deposits, and it demonstrates the importance of a careful examination of the mud layers in the environmental interpretation of such deposits. At the larger scale, it shows that a regressive coastal environment with stable sea level is not the only condition in which deltas can form, and that estuaries are not formed during every transgression.

REFERENCES CITED

Allen, G.P., and Posamentier, H.W., 1993, Sequence stratigraphy and facies model of an incised valley fill: The Gironde Estuary, France: Journal of Sedimentary Petrology, v. 63, p. 378–391.

Baas, J.H., Best, J.L., Peakall, J., and Wang, M., 2009, A phase diagram for turbulent, transitional, and laminar clay suspension flows: Journal of Sedimentary Research, v. 79, p. 162–183, doi:10.2110/jsr.2009.025.

Bard, E., Hamelin, B., and Delanghe-Sabatier, D., 2010, Deglacial meltwater pulse 1B and Younger Dryas sea levels revisited with boreholes at Tahiti: Science, v. 327, p. 1235–1237, doi:10.1126/science.1180557.

Berné, S., Vagner, P., Guichard, F., Lericolais, G., Liu, Z.X., Trentesaux, A., Yin, P., and Yi, H.I., 2002, Pleistocene forced regressions and tidal sand ridges in the East China Sea: Marine Geology, v. 188, p. 293–315, doi:10.1016/S0025-3227(02)00446-2.

Bhattacharya, J.P., 2010, Deltas, *in* James, N.P., and Dalrymple, R.W., eds., Facies Models 4: St. John's, Geological Association of Canada, p. 233–264.

Blott, S.J., and Pye, K., 2001, Gradistat: A grain size distribution and statistics package for the analysis of unconsolidated sediments: Earth Surface Processes and Landforms, v. 26, p. 1237–1248.

Blum, M.D., and Roberts, H.H., 2012, The Mississippi delta region: Past, present, and future: Annual Review of Earth and Planetary Sciences, v. 40, p. 655–683, doi:10.1146/annurev-earth-042711-105248.

Boyd, R., Suter, J., and Penland, S., 1989, Relation of sequence stratigraphy to modern sedimentary environments: Geology, v. 17, p. 926–929, doi:10.1130/0091-7613(1989)017<0926:ROSSTM>2.3.CO;2.

Boyd, R., Dalrymple, R.W., and Zaitlin, B.A., 2006, Estuarine and incised-valley facies models, *in* Posamentier, H.W., and Walker, R.G., eds., Facies Models Revisited: Society for Sedimentary Geology (SEPM) Special Publication 84, p. 171–235, doi:10.2110/pec.06.84.0171.

Catuneanu, O., 2006, Principles of Sequence Stratigraphy: Amsterdam, Netherlands, Elsevier, p. 105–159.

Chaumillon, E., and Weber, N., 2006, Spatial variability of modern incised valleys on the French Atlantic coast: Comparison between the Charente and the Lay-Sèvre incised valleys, *in* Dalrymple, R.W., Leckie, D.A., and Tillman, R.W., eds., Incised Valleys in Time and Space: Society for Sedimentary Geology (SEPM) Special Publication 85, p. 57–85, doi:10.2110/pec.06.85.0057.

Chen, J.Y., Shen, H.T., and Yun, C.X., 1988, Dynamic Processes and Morphological Evolution of Yangtze Estuary: Shanghai, China, Shanghai Science and Technology Press, 453 p. [in Chinese with English abstract].

Chen, S., Steel, R.J., and Olariu, C., 2015, Paleo-Orinoco (Pliocene) channels on the tide-dominated Morne L'Enfer delta lobes and estuaries, SW Trinidad, *in* Ashworth, P.J., Best, J.L., and Parsons, D.R., eds., Fluvial-Tidal Sedimentology: Amsterdam, Netherlands, Elsevier, Developments in Sedimentology 68, p. 227–281, doi:10.1016/B978-0-444-63529-7.00010-9.

Chen, S.L., Zhang, G.A., Yang, S.L., and Shi, J.Z., 2006, Temporal variations of fine suspended sediment concentration in the Changjiang River estuary and adjacent coastal waters, China: Journal of Hydrology (Amsterdam), v. 331, p. 137–145, doi:10.1016/j.jhydrol.2006.05.013.

Chen, Z.Y., and Stanley, D.J., 1995, Quaternary subsidence and river channel migration in the Yangtze delta plain, eastern China: Journal of Coastal Research, v. 11, p. 927–945.

Chen, Z.Y., Song, B.Q., Wang, Z.H., and Cai, Y.L., 2000, Late Quaternary evolution of the subaqueous Yangtze Delta, China: Sedimentation, stratigraphy, palynology, and deformation: Marine Geology, v. 162, p. 423–441, doi:10.1016/S0025-3227(99)00064-X.

Chen, Z.Y., Saito, Y., Hori, K., Zhao, Y.W., and Kitamura, A., 2003, Early Holocene mud-ridge formation in the Yangtze offshore, China: A tidal-controlled estuarine pattern and sea-level implications: Marine Geology, v. 198, p. 245–257, doi:10.1016/S0025-3227(03)00119-1.

Chen, Z.Y., Wang, Z.H., Schneiderman, J., Tao, J., and Cai, Y.L., 2005, Holocene climate fluctuations in the Yangtze delta of eastern China and the Neolithic response: The Holocene, v. 15, p. 915–924, doi:10.1191/0959683605hl862rr.

Cheng, H.Q., Kostaschuk, R., and Shi, Z., 2004, Tidal currents, bed sediments, and bedforms at the South Branch and the South Channel of the Changjiang (Yangtze) estuary, China: Implications for the ripple-dune transition: Estuaries, v. 27, p. 861–866, doi:10.1007/BF02912047.

Choi, K.S., Dalrymple, R.W., Chun, S.S., and Kim, S.P., 2004, Sedimentology of modern, inclined heterolithic stratification (IHS) in the macrotidal Han River delta, Korea: Journal of Sedimentary Research, v. 74, p. 677–689, doi:10.1306/030804740677.

Collinson, J.D., and Thompson, D.B., 1989, Sedimentary Structures: London, Unwin Hyman, 207 p.

Cummings, D.I., Dalrymple, R.W., Choi, K., and Jin, J.H., 2015, The Tide-Dominated Han River Delta, Korea: Geomorphology, Sedimentology, and Stratigraphic Architecture: Amsterdam, Netherlands, Elsevier, 376 p.

Dalrymple, R.W., 2010, Tidal depositional systems, *in* James, N.P., and Dalrymple, R.W., eds., Facies Models 4: St. John's, Newfoundland, Canada, Geological Association of Canada, p. 201–231.

Dalrymple, R.W., and Choi, K., 2007, Morphologic and facies trends through the fluvial-marine transition in tide-dominated depositional systems: A schematic framework for environmental and sequence-stratigraphic interpretation: Earth-Science Reviews, v. 81, p. 135–174, doi:10.1016/j.earscirev.2006.10.002.

Dalrymple, R.W., Zaitlin, B.A., and Boyd, R., 1992, Estuarine facies models: Conceptual basis and stratigraphic implications: Journal of Sedimentary Petrology, v. 62, p. 1130–1146, doi:10.1306/D4267A69-2B26-11D7-8648000102C1865D.

Dalrymple, R.W., Boyd, R., and Zaitlin, B.A., 1994, History of research, types and internal organization of incised-valley systems: Introduction to the volume, *in* Dalrymple, R.W., Boyd, R., and Zaitlin, B.A., eds., Incised-Valley Systems: Origin and Sedimentary Sequences: Society for Sedimentary Geology (SEPM) Special Publication 51, p. 3–10.

Dalrymple, R.W., Baker, E.K., Harris, P.T., and Hughes, M.G., 2003, Sedimentology and stratigraphy of a tide-dominated, foreland-basin delta (Fly River, Papua New Guinea), *in* Sidi, F.H., Nummedal, D., Imbert, P., Darman, H., and Posamentier, H.W., eds., Tropical Deltas of Southeast Asia-Sedimentology, Stratigraphy, and Petroleum Geology: Society for Sedimentary Geology (SEPM) Special Publication 76, p. 147–173, doi:10.2110/pec.03.76.0147.

Dalrymple, R.W., Mackay, D.A., Ichaso, A.A., and Choi, K.S., 2012, Processes, morphodynamics, and facies of tide-dominated estuaries, *in* Davis, R.A., Jr., and Dalrymple, R.W., eds., Principles of Tidal Sedimentology: New York, Springer, p. 79–107, doi:10.1007/978-94-007-0123-6_5.

Dalrymple, R.W., Kurcinka, C.E., Jablonski, B.V.J., Ichaso, A.A., and Mackay, D.A., 2015, Deciphering the relative importance of fluvial and tidal processes in the fluvial-marine transition, *in* Ashworth, P.J., Best, J.L., and Parsons, D.R., eds., Fluvial-Tidal Sedimentology: Amsterdam, Netherlands, Elsevier, Developments in Sedimentology 68, p. 3–45, doi:10.1016/B978-0-444-63529-7.00002-X.

Deschamps, P., Durand, N., Bard, E., Hamelin, B., Camoin, G., Thomas, A.L., Henderson, G.M., Okuno, J., and Yokoyama, Y., 2012, Ice-sheet collapse and sea-level rise at the Bolling warming 14,600 years ago: Nature, v. 483, p. 559–564, doi:10.1038/nature10902.

Doxaran, D., Froidefond, J.M., Castaing, P., and Babin, M., 2009, Dynamics of the turbidity maximum zone in a macrotidal estuary (the Gironde, France): Observations from field and MODIS satellite data: Estuarine, Coastal and Shelf Science, v. 81, p. 321–332, doi:10.1016/j.ecss.2008.11.013.

Fairbanks, R.G., 1989, A 17,000-year glacio-eustatic sea level record: Influence of glacial melting rates on the Younger Dryas event and deep-ocean circulation: Nature, v. 342, p. 637–642, doi:10.1038/342637a0.

Fan, D.D., and Li, C.X., 2002, Rhythmic deposition on mudflats in the mesotidal Changjiang estuary, China: Journal of Sedimentary Research, v. 72, p. 543–551, doi:10.1306/112901720543.

Fan, D.D., Li, C.X., Wang, D.J., Wang, P., Archer, A.W., and Greb, S.F., 2004, Morphology and sedimentation on open-coast intertidal flats of the Changjiang delta, China: Journal of Coastal Research, v. 43, p. 23–35.

Fan, D.D., Guo, Y.X., Wang, P., and Shi, J.Z., 2006, Cross-shore variations in morphodynamic processes of an open-coast mudflat in the Changjiang delta, China: With an emphasis on storm impacts: Continental Shelf Research, v. 26, p. 517–538, doi:10.1016/j.csr.2005.12.011.

Fan, D.J., Qi, H.Y., Sun, X.X., Liu, Y., and Yang, Z.S., 2011, Annual lamination and its sedimentary implications in the Yangtze River delta inferred from high-resolution biogenic silica and sensitive grain-size records: Continental Shelf Research, v. 31, p. 129–137, doi:10.1016/j.csr.2010.12.001.

Feldman, H., and Demko, T., 2015, Recognition and prediction of petroleum reservoirs in the fluvial/tidal transition, *in* Ashworth, P.J., Best, J.L., and Parsons, D.R., eds., Fluvial-Tidal Sedimentology: Amsterdam, Netherlands, Elsevier, Developments in Sedimentology 68, p. 483–528, doi:10.1016/B978-0-444-63529-7.00014-6.

Feng, Z.B., Liu, B.H., Zhao, Y.X., Li, X.H., Jiang, L., and Si, S.K., 2016, Spatial and temporal variations and controlling factors of sediment accumulation in the Yangtze River estuary and its adjacent sea area in the Holocene, especially in the early Holocene: Continental Shelf Research, v. 125, p. 1–17, doi:10.1016/j.csr.2016.06.007.

Fisk, H.N., and McFarlan, E., Jr., 1955, Late Quaternary deltaic deposits of the Mississippi River—Local sedimentation and basin tectonics, *in* Poldervaart, A., ed., Crust of the Earth: Geological Society of America Special Paper 62, p. 279–302.

Gabioux, M., Vinzon, S.B., and Paiva, A.M., 2005, Tidal propagation over fluid mud layers on the Amazon Shelf: Continental Shelf Research, v. 25, p. 113–125, doi:10.1016/j.csr.2004.09.001.

Gastaldo, R.A., Allen, G.P., and Huc, A.Y., 1995, The tidal character of fluvial sediments of the modern Mahakam River delta, Kalimantan, Indonesia, *in* Flemming, B.W., and Bartholoma, A., eds., Tidal Signatures in Modern and Ancient Sediments: International Association of Sedimentologists Special Publication 24, p. 171–181, doi:10.1002/9781444304138.ch11.

Goodbred, S.L., Jr., and Kuehl, S.A., 2000a, The significance of large sediment supply, active tectonism, and eustasy on margin sequence development: Late Quaternary stratigraphy and evolution of the Ganges-Brahmaputra delta: Sedimentary Geology, v. 133, p. 227–248, doi:10.1016/S0037-0738(00)00041-5.

Goodbred, S.L., Jr., and Kuehl, S.A., 2000b, Enormous Ganges-Brahmaputra sediment discharge during strengthened early Holocene monsoon: Geology, v. 28, p. 1083–1086, doi:10.1130/0091-7613(2000)28<1083:EGSDDS>2.0.CO;2.

Goodbred, S.L., Jr., and Saito, Y., 2012, Tide-dominated deltas, *in* Davis, Jr., R.A., and Dalrymple, R.W., eds., Principles of Tidal Sedimentology: New York, Springer, p. 129–149, doi:10.1007/978-94-007-0123-6_7.

Gu, H.L., and Wang, Q.S., 1989, Non-marine gastropod fossils of the Upper Cretaceous Taizhou formation from Haian area, north Jiangsu, *in* The Institute of Geological Sciences of Jiangsu Petroleum Exploration Bureau, ed., Stratigraphy and Palaeontology of the Taizhou Formation and the First Member of the Funing Formation, North Jiangsu Basin: Nanjing, China, Nanjing University Press, p. 155–183 [in Chinese with English abstract].

Hale, R.P., and Ogston, A.S., 2015, In situ observations of wave-supported fluid-mud generation and deposition on an active continental margin: Journal of Geophysical Research–Earth Surface, v. 120, p. 2357–2373, doi:10.1002/2015JF003630.

He, Q., Li, J.F., Li, Y., Jin, X.S., and Che, Y., 2001, Field measurements of bottom boundary layer processes and sediment resuspension in the Changjiang estuary: Science in China, ser. B, v. 44, p. 80–86, doi:10.1007/BF02884812.

Hijma, M.P., and Cohen, K.M., 2010, Timing and magnitude of the sea-level jump preluding the 8200 yr event: Geology, v. 38, p. 275–278, doi:10.1130/G30439.1.

Hill, P.L., Fox, J.M., Crockett, J.S., Curran, K.J., Friedrichs, C.T., Geyer, W.R., Milligan, T.G., Ogston, A.S., Puig, P., Scully, M.E., Traykovski, P.A., and Wheatcroft, R.A., 2007, Sediment delivery to the seabed on continental margins, *in* Nittrouer, C.A., Austin, J.A., Field, M.E., Kravitz, J.H., Syvitski, J.P.M., and Wiberg, P.L., eds., Continental Margin Sedimentation: From Sediment Transport to Sequence Stratigraphy: International Association of Sedimentologists Special Publication 37, p. 49–99.

Hori, K., and Saito, Y., 2007, An early Holocene sea-level jump and delta initiation: Geophysical Research Letters, v. 34, 2007, doi:10.1029/2007GL031029.

Hori, K., Saito, Y., Zhao, Q.H., Cheng, X.R., Wang, P.X., Sato, Y., and Li, C.X., 2001a, Sedimentary facies of the tide-dominated paleo-Changjiang (Yangtze) estuary during the last transgression: Marine Geology, v. 177, p. 331–351, doi:10.1016/S0025-3227(01)00165-7.

Hori, K., Saito, Y., Zhao, Q.H., Cheng, X.R., Wang, P.X., Sato, Y., and Li, C.X., 2001b, Sedimentary facies and Holocene progradation rates of the Changjiang (Yangtze) delta, China: Geomorphology, v. 41, p. 233–248, doi:10.1016/S0169-555X(01)00119-2.

Hori, K., Saito, Y., Zhao, Q.H., and Wang, P.X., 2002a, Evolution of the coastal depositional systems of the Changjiang (Yangtze) River in response to late Pleistocene–Holocene sea-level changes: Journal of Sedimentary Research, v. 72, p. 884–897, doi:10.1306/052002720884.

Hori, K., Saito, Y., Zhao, Q.H., and Wang, P.X., 2002b, Architecture and evolution of the tide-dominated Changjiang (Yangtze) River delta, China: Sedimentary Geology, v. 146, p. 249–264, doi:10.1016/S0037-0738(01)00122-1.

Hori, K., Saito, Y., Zhao, Q., and Wang, P., 2002c, Control of incised-valley fill stacking patterns by accelerated and decelerated sea-level rise: The Changjiang example during the last deglaciation: Geo-Marine Letters, v. 22, p. 127–132, doi:10.1007/s00367-002-0105-y.

Ichaso, A.A., and Dalrymple, R.W., 2009, Tide- and wave-generated fluid mud deposits in the Tilje Formation (Jurassic), offshore Norway: Geology, v. 37, p. 539–542, doi:10.1130/G25481A.1.

Ichaso, A.A., and Dalrymple, R.W., 2014, Eustatic, tectonic and climatic controls on an early syn-rift mixed-energy delta, Tilje Formation (Early Jurassic, Smørbukk Field, offshore mid-Norway), *in* Martinius, A.W., Ravnås, R., Howell, J.A., Steel, R.J., and Wonham, J.P., eds., From Depositional Systems to Sedimentary Successions on the Norwegian Continental Margin: International Association of Sedimentologists Special Publication 46, p. 339–388.

Ichaso, A.A., Dalrymple, R.W., and Martinius, A.W., 2016, Basin analysis and sequence stratigraphy of the synrift Tilje Formation (Lower Jurassic), Haltern terrace giant oil and gas fields, offshore mid-Norway: American Association of Petroleum Geologists Bulletin, v. 100, p. 1329–1375, doi:10.1306/02251614081.

Jablonski, B.V.J., and Dalrymple, R.W., 2016, Recognition of strong seasonality and climatic cyclicity in an ancient fluvially dominated, tidally influenced point bar: Middle McMurray Formation, Lower Steepbank River, north-eastern Alberta, Canada: Sedimentology, v. 63, p. 552–585, doi:10.1111/sed.12228.

Jaeger, J.M., and Nittrouer, C.A., 1995, Tidal controls on the formation of fine-scale sedimentary strata near the Amazon River mouth: Marine Geology, v. 125, p. 259–281, doi:10.1016/0025-3227(95)00015-Q.

Kineke, G.C., Sternberg, R.W., Trowbridge, J.H., and Geyer, W.R., 1996, Fluid-mud processes on the Amazon continental shelf: Continental Shelf Research, v. 16, p. 667–696, doi:10.1016/0278-4343(95)00050-X.

Kirby, R., and Parker, W.R., 1983, Distribution and behavior of fine sediment in the Severn Estuary and inner Bristol Channel, U.K.: Canadian Journal of Fisheries and Aquatic Sciences, v. 40, p. 83–95, doi:10.1139/f83-271.

Koutavas, A., Lynch-Stieglitz, J., Marchitto, T.M., Jr., and Sachs, J.P., 2002, El Niño–like pattern in ice age tropical Pacific sea surface temperature: Science, v. 297, p. 226–230, doi:10.1126/science.1072376.

Kuehl, S.A., Nittrouer, C.A., Allison, M.A., Faria, L.E.C., Dukat, D.A., Jaeger, J.M., Pacioni, T.D., Figueiredo, A.G., and Underkoffler, E.C., 1996, Sediment deposition, accumulation, and seabed dynamics in an energetic fine-grained coastal environment: Continental Shelf Research, v. 16, p. 787–815, doi:10.1016/0278-4343(95)00047-X.

Legler, B., Johnson, H.D., Hampson, G.J., Massart, B.Y.G., Jackson, C.A.L., Jackson, M.D., El-Barkooky, A., and Ravnas, R., 2013, Facies model of a fine-grained, tide-dominated delta: Lower Dir Abu Lifa Member (Eocene), Western Desert, Egypt: Sedimentology, v. 60, p. 1313–1356, doi:10.1111/sed.12037.

Li, C.X., and Wang, P.X., 1998, Late Quaternary Stratigraphy of the Yangtze Delta: Beijing, China Science Press, 222 p. [in Chinese].

Li, C.X., Li, P., and Chen, X.R., 1983, The influence of marine factors on sedimentary characteristics of Yangtze River channel below Zhenjiang: Acta Geographica Sinica, v. 50, p. 128–140 [in Chinese with English abstract].

Li, C.X., Chen, Q.Q., Zhang, J.Q., Yang, S.Y., and Fan, D.D., 2000, Stratigraphy and paleoenvironmental changes in the Yangtze delta during the late Quaternary: Journal of Asian Earth Sciences, v. 18, p. 453–469, doi:10.1016/S1367-9120(99)00078-4.

Li, C.X., Wang, P., Sun, H.P., Zhang, J.Q., Fan, D.D., and Deng, B., 2002, Late Quaternary incised-valley fill of the Yangtze delta (China): Its stratigraphic framework and evolution: Sedimentary Geology, v. 152, p. 133–158, doi:10.1016/S0037-0738(02)00066-0.

Li, C.X., Wang, P., Fan, D.D., and Yang, S.Y., 2006, Characteristics and formation of late Quaternary incised-valley-fill sequences in sediment-rich deltas and estuaries: Case studies from China, *in* Dalrymple, R.W., Leckie, D.A., and Tillman, R.W., eds., Incised Valleys in Time and Space: Society for Sedimentary Geology (SEPM) Special Publication 85, p. 141–160, doi:10.2110/pec.06.85.0141.

Li, G.X., Li, P., Liu, Y., Qiao, L.L., Ma, Y.Y., Xu, J.S., and Yang, Z.G., 2014, Sedimentary system response to the global sea level change in the East China Seas since the Last Glacial Maximum: Earth-Science Reviews, v. 139, p. 390–405, doi:10.1016/j.earscirev.2014.09.007.

Li, J.F., and Zhang, C., 1998, Sediment resuspension and implications for turbidity maximum in the Changjiang estuary: Marine Geology, v. 148, p. 117–124, doi:10.1016/S0025-3227(98)00003-6.

Li, J.F., Shi, W.R., and Shen, H.T., 1994, Sediment properties and transportation in the turbidity maximum in Changjiang estuary: Geographical Research, v. 13, p. 51–59 [in Chinese with English abstract].

Li, J.F., Wan, X.N., Ying, M., and Chen, X.H., 2005, Field observations on bed sediments and sandwaves in Changjiang estuary: International Journal of Sediment Research, v. 20, p. 129–135.

Li, W.H., Cheng, H.Q., Li, J.F., and Dong, P., 2008, Temporal and spatial changes of dunes in the Changjiang (Yangtze) estuary, China: Estuarine, Coastal and Shelf Science, v. 77, p. 169–174, doi:10.1016/j.ecss.2007.09.006.

Lin, C.M., Gu, L.X., Li, G.Y., Zhao, Y.Y., and Jiang, W.S., 2004, Geology and formation mechanism of late Quaternary shallow biogenic gas reservoirs in the Hangzhou Bay area, eastern China: American Association of Petroleum Geologists Bulletin, v. 88, p. 613–625, doi:10.1306/01070403038.

Lin, C.M., Zhuo, H.C., and Gao, S., 2005, Sedimentary facies and evolution in the Qiantang River incised valley, eastern China: Marine Geology, v. 219, p. 235–259, doi:10.1016/j.margeo.2005.06.009.

Lin, C.M., Li, Y.L., Zhuo, H.C., Shurr, G.W., Ridgley, J.L., Zhang, Z.P., and Xue, T., 2010, Features and sealing mechanism of shallow biogenic gas in incised valley fills (the Qiantang River, eastern China): A case study: Marine and Petroleum Geology, v. 27, p. 909–922, doi:10.1016/j.marpetgeo.2009.11.006.

Lin, C.M., Zhang, X., Xu, Z.Y., Deng, C.W., Yin, Y., and Chen, Q.Q., 2015, Sedimentary characteristics and accumulation conditions of shallow-biogenic gas for the late Quaternary sediments in the Changjiang River delta area: Advances in Earth Science, v. 30, p. 589–601 [in Chinese with English abstract].

Liu, J., Saito, Y., Kong, X.H., Wang, H., Xiang, L.H., Wen, C., and Nakashima, R., 2010, Sedimentary record of environmental evolution off the Yangtze River estuary, East China Sea, during the last ~13,000 years, with special reference to the influence of the Yellow River on the Yangtze River delta during the last 600 years: Quaternary Science Reviews, v. 29, p. 2424–2438, doi:10.1016/j.quascirev.2010.06.016.

Liu, K.B., Sun, S.C., and Jiang, X.H., 1992, Environmental change in the Yangtze River delta since 12,000 years BP: Quaternary Research, v. 38, p. 32–45.

MacEachern, J.A., Pemberton, S.G., Gingras, M.K., and Bann, K.L., 2010, Ichnology and facies models, *in* James, N.P., and Dalrymple, R.W., eds., Facies Models 4: St. John's, Newfoundland, Canada, Geological Association of Canada, p. 19–58.

Mackay, D.A., and Dalrymple, R.W., 2011, Dynamic mud deposition in a tidal environment: The record of fluid-mud deposition in the Cretaceous Bluesky Formation, Alberta, Canada: Journal of Sedimentary Research, v. 81, p. 901–920, doi:10.2110/jsr.2011.74.

McCave, I.N., 1970, Deposition of fine-grained sediment from tidal currents: Journal of Geophysical Research, v. 75, p. 4151–4159, doi:10.1029/JC075i021p04151.

Milliman, J.D., and Syvitski, J.P.M., 1992, Geomorphic/tectonic control of sediment discharge to the ocean: The importance of small mountainous rivers: The Journal of Geology, v. 100, p. 525–544, doi:10.1086/629606.

Milliman, J.D., Shen, H.T., Yang, Z.S., and Meade, R.H., 1985, Transport and deposition of river sediment in the Changjiang estuary and adjacent continental shelf: Continental Shelf Research, v. 4, p. 37–45, doi:10.1016/0278-4343(85)90020-2.

Nittrouer, J.A., Mohrig, D., Allison, M.A., and Peyret, A.P.B., 2011, The lowermost Mississippi River: A mixed bedrock-alluvial channel: Sedimentology, v. 58, p. 1914–1934, doi:10.1111/j.1365-3091.2011.01245.x.

Olariu, C., Steel, R.J., Dalrymple, R.W., and Gingras, M.K., 2012, Tidal dunes versus tidal bars: The sedimentological and architectural characteristics of compound dunes in a tidal seaway, the lower Baronia sandstone (Lower Eocene), Ager Basin, Spain: Sedimentary Geology, v. 279, p. 134–155, doi:10.1016/j.sedgeo.2012.07.018.

Pemberton, S.G., MacEachern, J.A., and Frey, R.W., 1992, Trace fossil facies models: Environmental and allostratigraphic significance, *in* Walker, R.G., and James, N.P., eds., Facies Models: Response to Sea Level Change: St. John's, Newfoundland, Canada, Geological Association of Canada, p. 47–72.

Penland, S., Boyd, R., and Suter, J.R., 1988, Transgressive depositional systems of the Mississippi delta plain: A model for barrier shoreline and shelf sand development: Journal of Sedimentary Petrology, v. 58, p. 932–949.

Qian, N., 1990, Fluvial processes in the lower Yellow River after levee breaching at Tongwaxiang in 1855: International Journal of Sediment Research, v. 5, p. 1–13.

Reimer, P.J., Bard, E., Bayliss, A., Beck, J.W., Blackwell, P.G., Ramsey, C.B., Buck, C.E., Cheng, H., Edwards, R.L., Friedrich, M., Grootes, P.M., Guilderson, T.P., Haflidason, H., Hajdas, I., Hatté, C., Heaton, T.J., Hoffmann, D.L., Hogg, A.G., Hughen, K.A., Kaiser, K.F., Kromer, B., Manning, S.W., Niu, M., Reimer, R.W., Richards, D.A., Scott, E.M., Southon, J.R., Staff, R.A., Turney, C.S.M., and van der Plicht, J., 2013, IntCal13 and MARINE13 radiocarbon age calibration curves 0–50000 years cal BP: Radiocarbon, v. 55, p. 1869–1887, doi:10.2458/azu_js_rc.55.16947.

Rühlemann, C., Mulitza, S., Müller, P.J., Wefer, G., and Zahn, R., 1999, Warming of the tropical Atlantic Ocean and shutdown of thermohaline circulation during the last deglaciation: Nature, v. 402, p. 511–514, doi:10.1038/990069.

Schneiderman, J.S., Chen, J.S., and Eckert, J.O., Jr., 2003, Heavy minerals and river channel migration in the Yangtze delta plain, eastern China: Journal of Coastal Research, v. 19, p. 326–335.

Schrottke, K., Becker, M., Bartholoma, A., Flemming, B.W., and Hebbeln, D., 2006, Fluid mud dynamics in the Weser estuary turbidity zone tracked by high resolution side-scan sonar and parametric sub-bottom profiler: Geo-Marine Letters, v. 26, p. 185–198, doi:10.1007/s00367-006-0027-1.

Shen, H., Guo, C., Zhu, H., Xu, H., Yun, C., and Chen, B., 1988, A discussion on the change and origin of turbidity maximum in the Changjiang estuary, *in* Chen, J., Shen, H., and Yu, C., eds., Process of Dynamics and Geomorphology of the Changjiang Estuary: Shanghai, China, Shanghai Scientific and Technical Publishers, p. 216–228 [in Chinese].

Shen, H.T., and Pan, D.A., eds., 2001, Turbidity Maximum in the Changjiang Estuary: Beijing, China Ocean Press, 194 p. [in Chinese].

Shen, H.T., He, S.L., Pan, D.A., and Li, J.F., 1992, A study of turbidity maximum in the Changjiang estuary: Acta Geographica Sinica, v. 47, p. 472–479 [in Chinese with English abstract].

Shen, H.T., Mao, Z.C., and Zhu, J.R., 2003, Saltwater Intrusion in the Changjiang Estuary: Beijing, China Ocean Press, 175 p. [in Chinese].

Shi, J.Z., Zhang, S.Y., and Hamilton, L.J., 2006, Bottom fine sediment boundary layer and transport processes at the mouth of the Changjiang estuary, China: Journal of Hydrology (Amsterdam), v. 327, p. 276–288, doi:10.1016/j.jhydrol.2005.11.039.

Shi, Z., 2004, Behaviour of fine suspended sediment at the North passage of the Changjiang estuary, China: Journal of Hydrology (Amsterdam), v. 293, p. 180–190, doi:10.1016/j.jhydrol.2004.01.014.

Slingerland, R., and Smith, N.D., 2004, River avulsions and their deposits: Annual Review of Earth and Planetary Sciences, v. 32, p. 257–285, doi:10.1146/annurev.earth.32.101802.120201.

Song, B., Li, Z., Saito, Y., Okuno, J., Li, Z., Lu, A.Q., Hua, D., Li, J., Li, X.H., and Nakashima, R., 2013, Initiation of the Changjiang (Yangtze) delta and its response to the mid-Holocene sea level change: Palaeogeography, Palaeoclimatology, Palaeoecology, v. 388, p. 81–97, doi:10.1016/j.palaeo.2013.07.026.

Stanley, D.J., and Chen, Z.Y., 1996, Neolithic settlement distributions as a function of sea level–controlled topography in the Yangtze delta, China: Geology, v. 24, p. 1083–1086, doi:10.1130/0091-7613(1996)024<1083:NSDAAF>2.3.CO;2.

Stanley, D.J., and Warne, A.G., 1994, Worldwide initiation of Holocene marine deltas by deceleration of sea-level rise: Science, v. 265, p. 228–231, doi:10.1126/science.265.5169.228.

Tang, T.Y., 1996, Quaternary stratigraphy on the shelf of the East China Sea, *in* Yang, Z.G., and Lin, H.M., eds., Quaternary Stratigraphy in China and its International Correlation: Beijing, Geology Press, p. 56–75 [in Chinese].

Tao, J., Chen, M.T., and Xu, S.Y., 2006, A Holocene environmental record from the southern Yangtze River delta, eastern China: Palaeogeography, Palaeoclimatology, Palaeoecology, v. 230, p. 204–229, doi:10.1016/j.palaeo.2005.07.015.

Tessier, B., 2012, Stratigraphy of tide-dominated estuaries, *in* Davis, R.A., Jr., and Dalrymple, R.W., eds., Principles of Tidal Sedimentology: New York, Springer, p. 109–128, doi:10.1007/978-94-007-0123-6_6.

Thomas, M.A., and Anderson, J.B., 1994, Sea-level controls on the facies architecture of the Trinity/Sabine incised-valley system, Texas continental shelf, *in* Dalrymple, R.W., Boyd, R., and Zaitlin, B.A., eds., Incised-Valley Systems: Origin and Sedimentary Sequences: Society for Sedimentary Geology (SEPM) Special Publication 51, p. 63–82, doi:10.2110/pec.94.12.0063.

Tjallingii, R., Stattegger, K., Stocchi, P., Saito, Y., and Wetzel, A., 2014, Rapid flooding of the southern Vietnam shelf during the early to mid-Holocene: Journal of Quaternary Science, v. 29, p. 581–588, doi:10.1002/jqs.2731.

Traykovski, P., Geyer, W.R., Irish, J.D., and Lynch, J.F., 2000, The role of wave-induced density-driven fluid mud flows for cross-shelf transport on the Eel River continental shelf: Continental Shelf Research, v. 20, p. 2113–2140, doi:10.1016/S0278-4343(00)00071-6.

Uehara, K., Saito, Y., and Hori, K., 2002, Paleotidal regime in the Changjiang (Yangtze) estuary, the East China Sea, and the Yellow Sea at 6 ka and 10 ka estimated from a numerical model: Marine Geology, v. 183, p. 179–192, doi:10.1016/S0025-3227(01)00255-9.

van den Berg, J.H., Boersma, J.R., and van Gelder, A., 2007, Diagnostic sedimentary structures of the fluvial-tidal transition zone—Evidence from deposits of the Rhine and Meuse: Netherlands Journal of Geosciences, v. 86, p. 287–306.

Wang, M.Y., 1982, Shallow natural gas in the modern Changjiang delta area: Natural Gas Industry, v. 3, p. 3–9 [in Chinese].

Wang, P.X., Zhang, J.J., Zhao, Q.H., Min, Q.B., Bian, Y.H., Zheng, L.F., Cheng, X.R., and Chen, R.H., 1988, Foraminifera and Ostracod in Surface Sediments of the East China Sea: Beijing, China Ocean Press, 438 p. [in Chinese with English abstract].

Wang, X.Y., Guo, Q.M., and Li, B.H., 2014, Foraminiferal record of core DY03 at the southern Yangtze delta and its paleoenvironmental implications: Acta Palaeontologica Sinica, v. 53, p. 85–91 [in Chinese with English abstract].

Wang, Y., Zhang, Y.Z., Zou, X.Q., Zhu, D.K., and Piper, D., 2012b, The sand ridge field of the South Yellow Sea: Origin by river-sea interaction: Marine Geology, v. 291–294, p. 132–146, doi:10.1016/j.margeo.2011.01.001.

Wang, Z.H., Saito, Y., Hori, K., Kitamura, A., and Chen, Z.Y., 2005, Yangtze offshore, China: Highly laminated sediments from the transition zone between subaqueous delta and the continental shelf: Estuarine, Coastal and Shelf Science, v. 62, p. 161–168, doi:10.1016/j.ecss.2004.08.012.

Wang, Z.H., Chen, Z.Y., Chen, J., and Wei, Z.X., 2007, Seismic framework and the Holocene morphological evolution of the Changjiang River mouth, China: Geomorphology, v. 85, p. 237–248, doi:10.1016/j.geomorph.2006.03.022.

Wang, Z.H., Xu, H., Zhan, Q., Saito, Y., He, Z.F., Xie, J.L., Li, X., and Dong, Y.H., 2010, Lithological and palynological evidence of late Quaternary depositional environments in the subaqueous Yangtze delta, China: Quaternary Research, v. 73, p. 550–562, doi:10.1016/j.yqres.2009.11.001.

Wang, Z.H., Zhuang, C.C., Saito, Y., Chen, J., Zhan, Q., and Wang, X.D., 2012a, Early mid-Holocene sea-level change and coastal environmental response on the southern Yangtze delta plain, China: Implications for the rise of Neolithic culture: Quaternary Science Reviews, v. 35, p. 51–62, doi:10.1016/j.quascirev.2012.01.005.

Wellner, R.W., and Bartek, L.R., 2003, The effect of sea level, climate, and shelf physiography on the development of incised-valley complexes: A modern example from the East China Sea: Journal of Sedimentary Research, v. 73, p. 926–940, doi:10.1306/041603730926.

Winkler, M.G., and Wang, P.K., 1993, The late Quaternary vegetation and climate of China, *in* Wright, H.E., Jr., Kutzbach, J.E., Webb, T., III, Ruddiman, W.F., Street-Perrott, F.A., and Bartlein, P.J., eds., Global Climates Since the Last Glacial Maximum: Minneapolis, Minnesota, University of Minnesota Press, p. 221–264.

Wu, J.X., Wang, Y.H., and Cheng, H.Q., 2009, Bedforms and bed material transport pathways in the Changjiang (Yangtze) estuary: Geomorphology, v. 104, p. 175–184, doi:10.1016/j.geomorph.2008.08.011.

Wu, J.X., Liu, J.T., and Wang, X., 2012, Sediment trapping of turbidity maxima in the Changjiang estuary: Marine Geology, v. 303–306, p. 14–25, doi:10.1016/j.margeo.2012.02.011.

Wu, S.H., Cheng, H.Q., Xu, Y.J., Li, J.F., Zheng, S.W., and Wei, X., 2016, Riverbed micromorphology of the Yangtze River estuary, China: Water (Basel), v. 8, doi:10.3390/w8050190.

Xu, S.Y., Shao, X.S., Chen, Z.Y., and Yan, Q.S., 1990, Storm deposits in the Changjiang delta: Science in China, ser. B, v. 33, p. 1242–1250.

Xu, T.Y., Wang, G.Q., Shi, X.F., Wang, X., Yao, Z.Q., Yang, G., Fang, X.S., Qiao, S.Q., Liu, S.F., Wang, X.C., and Zhao, Q.H., 2016, Sequence stratigraphy of the subaqueous Changjiang (Yangtze River) delta since the Last Glacial Maximum: Sedimentary Geology, v. 331, p. 132–147, doi:10.1016/j.sedgeo.2015.10.014.

Yang, S.L., and Yang, H.F., 2015, Temporal variations in water and sediment discharge from the Changjiang (Yangtze River) and downstream sedimentary response, *in* Zhang, J., ed., Ecological Continuum from the Changjiang (Yangtze River) Watersheds to the East China Sea Continental Margin: New York, Springer, p. 71–91, doi:10.1007/978-3-319-16339-0_4.

Yang, Y.P., Li, Y.T., Sun, Z.H., and Fan, Y.Y., 2014, Suspended sediment load in the turbidity maximum zone at the Yangtze River estuary: The trends and causes: Journal of Geographical Sciences, v. 24, p. 129–142, doi:10.1007/s11442-014-1077-3.

Yi, S., Saito, Y., and Yang, D.Y., 2006, Palynological evidence for Holocene environmental change in the Changjiang (Yangtze River) delta, China: Palaeogeography, Palaeoclimatology, Palaeoecology, v. 241, p. 103–117, doi:10.1016/j.palaeo.2006.06.016.

Yoneda, M., Uno, H., Shibata, Y., Suzuki, R., Kumamoto, Y., Yoshida, K., Sasaki, T., Suzuki, A., and Kawahata, H., 2007, Radiocarbon marine reservoir ages in the western Pacific estimated by pre-bomb molluscan shells: Nuclear Instruments and Methods in Physics Research B: Beam Interactions with Materials and Atoms, v. 259, p. 432–437.

Yu, W., Wang, H.J., and Li, Z.S., 1963, Gastropod Fossils in China: Beijing, Science Press, 437 p. [in Chinese].

Zhang, X., Lin, C.M., Li, Y.L., Qu, C.W., and Wang, S.J., 2013, Sealing mechanism for cap beds of shallow-biogenic gas reservoirs in the Qiantang River incised valley, China: Continental Shelf Research, v. 69, p. 155–167, doi:10.1016/j.csr.2013.09.006.

Zhang, X., Lin, C.M., Dalrymple, R.W., Gao, S., and Li, Y.L., 2014, Facies architecture and depositional model of a macrotidal incised-valley succession (Qiantang River estuary, eastern China), and differences from other macrotidal systems: Geological Society of America Bulletin, v. 126, p. 499–522.

Zhang, X., Dalrymple, R.W., Yang, S.Y., Lin, C.M., and Wang, P., 2015, Provenance of Holocene sediments in the outer part of the paleo–Qiantang River estuary, China: Marine Geology, v. 366, p. 1–15, doi:10.1016/j.margeo.2015.04.008.

Zhao, O., 1992, *Tulotomoides terrassa* and its relation to the accumulation of oil and gas: Acta Petrolei Sinica, v. 13, p. 47–50.

Zheng, K.F., 1998, Distribution and exploration prospects of the shallow gas in the Quaternary in Jiangsu Province: Natural Gas Industry, v. 18, p. 20–24 [in Chinese with English abstract].

Zhou, C.X., 1993, On sand-waves in Yawosha channel of the Yangtze estuary, *in* Proceedings of the Second International Symposium on River Sedimentation: Beijing, Water Resources and Electric Power Press, p. 650–661.

Zhou, X.J., and Gao, S., 2004, Spatial variability and representation of seabed sediment grain sizes: An example from the Zhoushan-Jinshanwei transect, Hangzhou Bay, China: Chinese Science Bulletin, v. 49, p. 2503–2507.

Zhu, H., Yun, C., Mao, Z., and Wang, S., 1988, Characteristics and empiric relationships of wind generated waves in the Changjiang estuary, *in* Chen, J., Shen, H., and Yu, C., eds., Process of Dynamics and Geomorphology of the Changjiang Estuary: Shanghai, China, Shanghai Scientific and Technical Publishers, p. 166–177 [in Chinese].

Zhu, Y.Q., Li, C.Y., Zeng, C.K., and Li, B.G., 1979, Lowest sea level of the continental shelf of the East China Sea in the late Pleistocene: Chinese Science Bulletin, v. 24, p. 317–320 [in Chinese].

Zhu, Y.Q., Zheng, C.K., and Feng, Y., 1984, The shelf geomorphic features of the East China Sea: Donghai Marine Science, v. 2, p. 1–13 [in Chinese with English abstract].